


# Discrete spectral eigenmode-resonance network of brain dynamics and connectivity

P. A. Robinson 

*School of Physics, University of Sydney, New South Wales 2006, Australia  
and Center for Integrative Brain Function, University of Sydney, New South Wales 2006, Australia*



(Received 6 May 2021; accepted 2 September 2021; published 20 September 2021)

The problem of finding a compact natural representation of brain dynamics and connectivity is addressed using an expansion in terms of physical spatial eigenmodes and their frequency resonances. It is demonstrated that this discrete expansion via the system transfer function enables linear and nonlinear dynamics to be analyzed in compact form in terms of natural dynamic “atoms,” each of which is a frequency resonance of an eigenmode. Because these modal resonances are determined by the system dynamics, not the investigator, they are privileged over widely used phenomenological patterns, and obviate the need for artificial discretizations and thresholding in coordinate space. It is shown that modal resonances participate as nodes of a discrete spectral network, are noninteracting in the linear regime, but are linked nonlinearly by wave-wave coalescence and decay processes. The modal resonance formulation is shown to be capable of speeding numerical calculations of strongly nonlinear interactions. Recent work in brain dynamics, especially based on neural field theory (NFT) approaches, allows eigenmodes and their resonances to be estimated from data without assuming a specific brain model. This means that dynamic equations can be inferred using system identification methods from control theory, rather than being assumed, and resonances can be interpreted as control-systems data filters. The results link brain activity and connectivity with control-systems functions such as prediction and attention via gain control and can also be linked to specific NFT predictions if desired, thereby providing a convenient bridge between physiologically based theories and experiment. Amplitudes of modes and resonances can also be tracked to provide a more direct and temporally localized representation of the dynamics than correlations and covariances, which are widely used in the field. By synthesizing many different lines of research, this work provides a way to link quantitative electrophysiological and imaging measurements, connectivity, brain dynamics, and function. This underlines the need to move between coordinate and spectral representations as required. Moreover, standard theoretical-physics approaches and mathematical methods can be used in place of ad hoc statistical measures such as those based on graph theory of artificially discretized and decimated networks, which are highly prone to selection effects and artifacts.

DOI: [10.1103/PhysRevE.104.034411](https://doi.org/10.1103/PhysRevE.104.034411)

## I. INTRODUCTION

Relationships between brain activity and structure are central to understanding how the brain functions and to interrelating and predicting experimental measurements. Tractability and interpretability of analyses require compact representations of these quantities and these are widely sought in the field, chiefly by statistical means and using approaches such as graph theory. The purpose of this paper is to obtain a compact representation from a physical starting point, which yields a description in terms of natural dynamical entities that embody spatial patterns and spectral resonances, rather than phenomenological or statistical constructs. This provides a bridge between experimentally observed spatiotemporal characteristics on one hand and corresponding predictions from physiologically based theories on the other, notably neural field theory (NFT).

At the microscopic level, the brain comprises a discrete network of around  $10^{11}$  neurons, each typically connected to  $10^3$ – $10^4$  others [1,2]. However, this level of descrip-

tion is unwieldy for analysis, computation, or comparison with large-scale mammalian brain dynamics and connectivity, notwithstanding large-scale efforts in this direction [3–5] and successes in smaller nervous systems such as that of *Caenorhabditis elegans* [6,7].

In recent years, much work has been done to study static and dynamic brain connectivity on scales up to and including the whole brain, with a literature now running to thousands of publications. At this scale, individual neurons are not resolved and brain tissue is effectively continuous. In most cases, structural and functional studies have involved discretizing or *parcellating* the brain into so-called *regions of interest* in coordinate space. Connectivities between these discretized regions are then quantified by tracing axonal connections or evaluating two-point correlation functions of brain activity or similar measures [6,8–11]. In both cases, the result is often expressed as a connection matrix (CM) of structural (i.e., axonal) or functional (i.e., correlation-based) connections between regions, which label the rows and columns.

Numerous methodological and analysis issues arise when discrete methods are applied to the continuous (at millimeter scales and above, where individual neurons are not resolved) brain, as discussed in detail in Ref. [12]. For example, there

\*robinson@physics.usyd.edu.au

is widespread disagreement over whether to parcellate based on known anatomical or functional subdivisions of the brain such as Brodmann areas, into equal-sized elements (typically of order a centimeter in linear size) that do not presuppose what the subdivisions should be and which avoid artifacts due to widely different regional sizes, or on some other basis [9,13–21]. Second, experimental CMs can contain  $10^4$ – $10^8$  elements, which makes them unwieldy and difficult to analyze. Tied to this is a widespread desire to exploit the isomorphism between CMs and corresponding graphs, in which each row and column of a CM represents a graph node and each entry is the strength of the corresponding edge [6,7,12,19]. Such graphs are extremely dense, so CMs are often severely thresholded to sparsify them by retaining only the largest entries and even binarizing the resulting matrix [16,17,19,22–24], thereby discarding much of its information content. Then statistics of discrete graph-theoretic quantities such as degree, centrality, and stepwise path length are calculated for the residual decimated structure [6,17,25]. Unfortunately, this represents a severe category error—no such macroscopically discrete structure exists within the cortex, for example, although structures such as thalamic nuclei and basal ganglia are discrete from one another; this is despite the existence of localized functions and other nonuniformities, because the projections of white matter tracts have significant spread. Many resulting measures are thus dominated by artifacts of the discretization and thresholding choices made [12,19,22,23], although some can be redefined to be valid in the limit of sufficiently fine discretization without thresholding [12]. Additionally, because the brain is near-critical, arbitrary removal of even relatively weak connections is questionable because it may significantly change criticality [26–32].

The above debates and inconsistencies have led to an explosion in the number of proposed analysis methods and measures and an extremely complex resulting literature. As a result it is often difficult or impossible to compare the results of different studies [19,22,23,33,34], although case-control comparisons within a single protocol can yield robust statistical differences between conditions, albeit without relating these quantitatively to underlying mechanisms.

A common source of difficulty in current analyses of brain connectivity and dynamics arises from discretizing the system in coordinate space (which is intrinsically complex and unwieldy) rather than in the spectral domain (which is straightforward in the linear regime). When subsequent thresholding and other ad hoc analysis steps are imposed to try to enforce a simple outcome by fiat, the difficulty can lead to errors in cases where interpretation is carried out through the lens of a presumed architecture (e.g., modular, small world, hierarchical) which is then enforced by bespoke analysis methods. Many problems thus arise from the widespread insistence on treating the large scale structure of the brain as if it really were the discrete system defined by the particular parcellation and thresholding/decimation chosen by an individual investigator, rather than viewing each parcellation as an approximate discretization of the macroscopically continuous system at hand. This is analogous to coarsely discretizing a structure such as a musical instrument or machine part, keeping only a few of the strongest connections between points,

and then studying the results by tabulating statistics of the discretization, rather than via relevant physical laws. By its very nature, such an approach is unlikely to yield first-principles understanding of system properties. Valid results depend on having a fine discretization, retaining connections, and using dynamical methods that are based on the physical properties of the system.

In recent years, much effort has gone into trying to detect patterns in brain connectivity and activity, mainly by using statistical means such as independent component analysis (ICA), principal component analysis (PCA), or  $k$ -means clustering of covariance patterns [35–38] to obtain phenomenological “resting-state networks” (RSNs) or other patterns without reference to the underlying dynamics [39,40]. Many of these approaches require by fiat that patterns be mutually exclusive with sharp edges [35,37,41].

Use of natural physical eigenmodes to analyze brain activity (in direct analogy to Fourier analysis of the dynamics of a violin string, for example) has a longer history and has the advantage that it relates any observed activity patterns to the dynamics of the brain [42–46]. More recently, it has also been used to analyze brain connectivity and express it in compact form within a NFT framework [47–51]. Graph-theoretic analogs have also been proposed [24,33,52,53]; unfortunately, some such studies suffer from overly coarse discretization, binarization and thresholding, and oversimplifications such as trying to explain individually selected patterns with a single “best” mode, without providing a rationale for ignoring the other patterns present and/or other modes [24,53]. In contrast, compact modal representations of dynamics and connectivity can be obtained if justified on a physical basis, consistently with known properties of inputs, neurodynamics, and modal structure [45,54]. Other successes of discrete approaches, especially those based on patterns, may result from use of methods that indirectly incorporate the contributions due to low-order eigenmodes without considering these modes explicitly [48].

Not only is the representation of activity in terms of the eigenfunction basis straightforward in the linear regime but CMs can also be represented compactly in terms of the same basis [8,49,50,55]. This can easily reduce a  $1000 \times 1000$  symmetric functional CM (fCM) with  $\sim 500\,000$  independent entries, to a diagonal matrix with 1000 entries, only a few tens of which are nonnegligible [47,50]. This achieves the widely desired aim of a compact, discrete representation in a systematic way; the price being that it is realized in the spectral domain, not coordinate space. However, this is not a major issue if one remembers the analogy with a violin string—each pure tone corresponds to a fixed sinusoidal spatial pattern that oscillates with an amplitude that can change over time [56]. Thus, as in other branches of physics, analyses of brain connectomics and dynamics need to switch between coordinate-space and spectral representations as required. Both representations are useful in different contexts, as in the analogous case of wave-particle duality in quantum physics—e.g., coordinate space for local neural interactions and spectral space for larger-scale phenomena.

Brain dynamics is more complex than that of a violin string, in which each spatial pattern has a unique frequency. In the brain, both experiment and NFT show that multiple

damped frequency resonances can exist for a single spatial pattern [29,56–60]. This aspect proves to be straightforward to handle using approaches from engineering control systems that approximate the transfer function of each mode as a rational function [61–64]. The result is a discrete sum of resonances that contribute to each mode's dynamics, each of which corresponds to a pole of the transfer function and has the properties of a proportional-integral-derivative (PID) data filter with potential cognitive roles such as prediction and attention [65]. Again, this provides a systematic means of truncating to obtain a finite representation with just a few poles retained for each of the dominant spatial modes. A key advantage of this method is that it represents the dynamics in terms of spatial patterns and spectral resonances that are widely observed experimentally and also predicted from specific physiologically based NFTs, thereby providing a convenient bridge between the two.

In almost all studies, connections between regions are treated as linear because axonal outputs are generally proportional to inputs, whereas local dynamics can be linear or nonlinear. In the linear regime, eigenmodes are noninteracting, which is what enables a very compact representation. However, large-scale brain activity can involve a variety of nonlinear effects, including firing rate responses, habituation, facilitation, and synaptic plasticity [66–68]. Nonlinear interactions have the effect of coupling the linear modes, an effect that can be treated either directly or by retaining additional terms in a perturbation expansion in the amplitude of the activity [69]. This is directly analogous to the situation in nonlinear optics and nonlinear plasma physics, where such expansions are standard [70–72]. So long as the interaction is not too strong, use of eigenmodes as the basis of expansion still yields a compact treatment of the dynamics, with the leading nonlinear terms describing three-wave coalescence and decay [70–72].

Wave-wave interactions have been widely observed in the brain in many contexts, including: (i) second-harmonic generation via three-wave coalescence of resonant alpha or spindle waves [69,73,74]; (ii) modulation of high-frequency waves such as  $\sim 40$  Hz gamma oscillations by lower-frequency ones, including slow-wave ( $\sim 1$  Hz), theta ( $\sim 4$  Hz), alpha ( $\sim 10$  Hz), and beta ( $\sim 20$  Hz) [26,75–84] ones; and (iii) three-wave coalescence and decay interactions seen in steady-state visual evoked potential experiments [85–87]. NFT perturbation expansions and simulations have accounted for a number of features of such phenomena [67,73,86,87]. Such interactions have also been postulated to play roles in neural processing and communication between areas—e.g., under the communication through coherence hypothesis that asserts that in-phase oscillations can enhance communication between neurons [76,81,84,88–103].

Here, our aim is to synthesize many prior lines of research from physics, engineering, and neuroscience to obtain a compact discrete representation of linear and moderately nonlinear brain dynamics and connectivity based on eigenmodes, resonances, and their interactions. We consider a broad class of NFT dynamical equations that follow macroscale activity by averaging over microscopic neural structure. The particular equations used here omit details to highlight the key features of this approach. We use a perturbation expansion in orders

of the external stimulus amplitude to express the dynamics in terms of a network of nonlinearly interacting modes. Further simplifications are then made by introducing a rational approximation to the modal transfer functions. The result is a set of solvable coupled-mode equations in coordinate space. Corresponding connection matrices between modes and resonances will thus be dominantly diagonal, with weaker off-diagonal terms arising from mode coupling. This formulation in terms of a discrete network of modal resonances achieves the aim of a compact, discrete representation of brain dynamics and connectivity in which each modal resonance is an interacting entity.

The structure of the paper is as follows. In Sec. II we introduce a neural field equation that is sufficiently general to establish the key results. Perturbation expansion of this equation is then carried out. Section III solves the perturbation equations to first order, deriving the linear transfer function and its eigenfunction expansion. A further expansion in terms of poles of the transfer function is then carried out to obtain equations for the amplitudes of the individual poles. Second-order nonlinear terms corresponding to three-wave interactions are analyzed in Sec. IV and expressed in terms of the modal linear transfer functions. How modal poles can speed numerical simulations of strongly nonlinear dynamics is then outlined in Sec. V. Section VI discusses some ways in which the interactions between modal resonances can be quantified. Section VII then describes procedures to obtain modes and poles from data and thereby avoid use of predetermined dynamic equations. The main results are summarized and discussed in Sec. VIII, where generalizations and future directions are also discussed.

## II. THEORY

In this section we introduce the class of neural field equations considered in the present work and expand their dynamics up to second order in external perturbations to the system. To keep the analysis as general as possible we do not adopt a specific NFT model of the underlying system and its nonlinearities, the aim being to establish the overall approach and overarching results.

### A. Neural field equation

A very wide range of brain activity dynamics can be described in terms of the mean firing rate of neurons  $Q(\mathbf{r}, t)$  as a function of the two-dimensional (2D) position  $\mathbf{r}$  on the cortex, and the time  $t$ . In the linear regime it is possible to write the firing rates of all neural populations—excitatory, inhibitory, and closely coupled thalamic ones, in terms of any one of the set [12,104]. Because excitatory neurons are primarily behind the signals detected in electroencephalography (EEG) and functional magnetic resonance imaging (fMRI) [42,105], we take  $Q$  to represent the mean excitatory firing rate henceforth. We do not consider the other populations explicitly because of our focus on the analysis of dynamics in terms of eigenmodes and resonances; however, these strongly influence the observable excitatory activity and are routinely incorporated into NFT models of the corticothalamic system, such as the ones cited in the Introduction and the next paragraph.

Neural field theory (NFT) averages over microscopic neural properties to obtain (in the present case) an equation of motion for  $Q(\mathbf{r}, t)$  when driven by external inputs  $N(\mathbf{r}, t)$ , which are mapped in a nearly one-to-one manner through the thalamus to the sensory cortex, with  $\mathbf{r}$  directly denoting position in the cortex and labeling the location connected to it in the thalamus (i.e., a rescaled position). A very wide class of such equations, whose predictions have been verified experimentally in many contexts, can be written in the form [42,48,104,106–122]

$$(D_t + D_r)Q(\mathbf{r}, t) = N(\mathbf{r}, t) + Z[Q(\mathbf{r}, t)], \quad (1)$$

where  $D_t$  and  $D_r$  are linear operators that depend only on time and position, respectively, and  $Z$  is a nonlinear function of  $Q$ . Typically,  $D_t$  describes the temporal dynamics that results locally from interactions within and between multiple neural populations and via topographically organized feedback loops between cortex and thalamus, including time delays during corticocortical and corticothalamic axonal propagation. The operator  $D_r$  describes spatial coupling via white matter connections; together with  $D_t$  it governs spatial propagation (across the cortex, for example) with associated spatial spreading and time delays. The quantity  $Z$  is approximated as being local in the present work but could involve integrals over different locations and times; its form is discussed further below.

An equivalent form to Eq. (1), without the nonlinear term, has been used in structural inference in geophysics, acoustics, and elsewhere [123], and includes wave and diffusion equations as special cases. This form also includes wide classes of equations in which the evolution of  $Q$  is driven by both local influences and integrated activity arriving from other locations—the kernel of the integral being the Green function of the dynamics [109].

Equations such as Eq. (1) can be solved by brute force numerical computation. However, our aim here is to understand the structure of the solutions and how they can be represented in terms of a naturally arising discrete network of modes and resonances. This will expose fundamental dynamic entities and their interactions in a form suitable to tackle a wide variety of problems in brain structure and dynamics.

### B. Perturbation expansion

Without loss of generality, we assume that

$$N(\mathbf{r}, t) = N^{(0)}(\mathbf{r}) + N^{(1)}(\mathbf{r}, t), \quad (2)$$

where  $N^{(0)}$  is the steady state value of  $N$  and  $N^{(1)}$  is a perturbation that represents the total time-varying external input.

We now expand Eq. (1) in orders of the perturbation by writing [67]

$$Q(\mathbf{r}, t) = Q^{(0)}(\mathbf{r}) + Q^{(1)}(\mathbf{r}, t) + Q^{(2)}(\mathbf{r}, t), \quad (3)$$

$$Z[Q(\mathbf{r}, t)] = Z^{(0)}[Q(\mathbf{r})] + Z^{(1)}[Q(\mathbf{r}, t)] + Z^{(2)}[Q(\mathbf{r}, t)], \quad (4)$$

where we have truncated the expansion at second order because many relevant nonlinearities occur at this order and it suffices to establish the key results. In this vein we also choose

the form

$$Z[Q(\mathbf{r}, t)] = a[Q(\mathbf{r}, t) - Q^{(0)}(\mathbf{r})]^2, \quad (5)$$

where  $a$  is a constant. This form represents a nonlinearity in the firing rate response to mean soma voltage in NFT, but other nonlinearities such as habituation, facilitation, and plasticity can be included in similar ways [66,67,69,87,107,122]. More generally, the firing rate nonlinearity is expected to be sigmoidal [124], leveling off at high and low  $Q$ , but Eq. (5) is a good approximation provided perturbations from the steady state do not become too large. Equations (4) and (5) imply

$$Z^{(0)}[Q(\mathbf{r})] = 0, \quad (6)$$

$$Z^{(1)}[Q(\mathbf{r}, t)] = 0, \quad (7)$$

$$Z^{(2)}[Q(\mathbf{r}, t)] = a[Q^{(1)}(\mathbf{r}, t)]^2. \quad (8)$$

Use of the form  $a[Q(\mathbf{r}, t)]^2$  on the right-hand side of Eq. (5) might seem simpler, but would lead to additional terms in Eqs. (6)–(8) that would complicate the subsequent analysis without affecting the conclusions except in detail.

Substitution of Eqs. (3)–(8) into Eq. (1) then yields

$$D_r Q^{(0)}(\mathbf{r}) = N^{(0)}(\mathbf{r}), \quad (9)$$

$$(D_t + D_r)Q^{(1)}(\mathbf{r}, t) = N^{(1)}(\mathbf{r}), \quad (10)$$

$$(D_t + D_r)Q^{(2)}(\mathbf{r}, t) = a[Q^{(1)}(\mathbf{r}, t)]^2, \quad (11)$$

where we have equated terms order by order.

## III. STEADY STATE, LINEAR RESPONSE, AND TRANSFER FUNCTION

In this section we first briefly summarize prior work on NFT linear dynamics and the system transfer function, including its expansion in terms of eigenfunctions. When applied to Eq. (1) these results yield a set of equations for the dynamics of each eigenmode, which we express in terms of transfer-function resonances, thereby leading to equations of motion for the contributions of the individual modal resonances to the overall dynamics.

### A. Steady state and linear dynamics

The steady state of the system is determined by solution of Eq. (9), which we do not need to examine explicitly here. Perturbations from this solution are what give rise to noninvasively measurable quantities such as EEG and fMRI signals [42,125].

The first-order perturbation  $Q^{(1)}$  is the solution of Eq. (10), which can be obtained by the standard method of separation of variables [126–128]. We start by solving in the case with  $N^{(1)} = 0$  by making the ansatz

$$Q^{(1)}(\mathbf{r}, t) = a(t)u(\mathbf{r}), \quad (12)$$

where the functions  $a(t)$  and  $u(\mathbf{r})$  depend only on the variables indicated and this separation is possible provided the structure of the system can be approximated as static on the timescale of variation of the activity. Substitution of this form into Eq. (10)



with  $N^{(1)} = 0$  and division by  $a(t)u(\mathbf{r})$  gives

$$\frac{D_t a(t)}{a(t)} = -\frac{D_r u(\mathbf{r})}{u(\mathbf{r})} = -K^2. \quad (13)$$

In this equation, we notice that the leftmost term is independent of  $\mathbf{r}$  and the middle term is independent of  $t$ ; since these are equal, they must both equal a common constant, written as  $-K^2$  on the right-hand side.

The above steps enable us to write the eigenfunction equation

$$D_r u(\mathbf{r}) = K^2 u(\mathbf{r}), \quad (14)$$

and the dispersion equation

$$D_t a(t) + K^2 a(t) = 0. \quad (15)$$

In applications, the eigenfunction equation is typically a spatial differential equation, which must be solved subject to the boundary conditions of the system. In bounded systems such as the brain, this gives rise to an eigenvalue spectrum in which  $K$  takes only discrete values  $K_j$ , with  $j = 0, 1, 2, \dots$  for corresponding spatial eigenfunctions  $u_j(\mathbf{r})$ . The  $u_j(\mathbf{r})$  can be normalized for symmetric  $D_r$  to form an orthonormal basis, with

$$\int u_j(\mathbf{r}) u_k(\mathbf{r}) d\mathbf{r} = \delta_{jk}, \quad (16)$$

where the integral is over all  $\mathbf{r}$  (in the present work integrals and sums written without bounds extend over the entire allowable domain),  $\delta_{jk}$  is a Kronecker delta, and we assume that the  $u_j(\mathbf{r})$  are real without loss of generality. Then any well-behaved function  $g(\mathbf{r})$  can be expressed in the form

$$g(\mathbf{r}) = \sum_j g_j u_j(\mathbf{r}), \quad (17)$$

$$g_j = \int u_j(\mathbf{r}) g(\mathbf{r}) d\mathbf{r}, \quad (18)$$

where the sum is over all modes. For example, if the operator  $D_r$  is the Laplacian, as is often a reasonable approximation [50,109], then Eq. (14) becomes the Helmholtz equation and the eigenfunctions are Fourier modes in 1D- and 2D-planar cases with wave number of magnitude  $K$  and spherical harmonics for the surface of a sphere [129]. The Laplacian approximation has been widely used in NFT (see references cited in the Introduction) but we do not make this approximation in the present work.

For  $K = K_j$  the dispersion Eq. (15) yields the corresponding temporal eigenfunction  $a_j(\omega)$ . The general solution of Eq. (10) is a sum of terms of the form  $a_j(t)u_j(\mathbf{r})$ .

In contrast to their dynamic role in the brain, eigenfunctions sometimes appear in the literature as descriptive tools to simplify the form of covariance matrices, graph structures, or other statistical measures [41,52], often relating to discretized and thresholded representations that are subject to the difficulties described above, and often postulating Laplacian spatial couplings without reference to physiology. Considerations of modal energies and eigenvalues that justify dominance of the lowest-order modes can only be made in a dynamical context [42,44,50,54,59].

At this point it is also worth noting that one must be careful to avoid well-known pitfalls when undertaking eigenfunction

expansion: (i) Just as in Fourier analysis, expansion of features with short length scales (e.g., narrow or sharp-edged patterns) leads to contributions from a broad spectrum of spatial eigenmodes owing to the spatial uncertainty principle, and the Gibbs phenomenon can also occur [127,128]. Phenomenological patterns such as RSNs are often forced to be mutually exclusive with sharp edges. This means that expansions of them in terms of eigenmodes will have artifactual tails of high-mode contributions that arise from the edges, which are prominent in the analysis in Ref. [24], for example. (ii) It is not appropriate to analyze patterns by finding the eigenmode with the “best match” to a single pattern selected from among many [24,53]—the chance of false positives is significant. In contrast, rigorous analysis requires avoidance of coarse discretization and thresholding, and evenhanded use of all significant eigenmodes; only then can extremely sparse representations of observed features sometimes be justified, as in Refs. [45,54], for example.

## B. Transfer function expansion in eigenfunctions

We can write Eq. (10) in the form [130]

$$Q^{(1)}(\mathbf{r}, t) = \iint T(\mathbf{r}, \mathbf{r}', t - t') N^{(1)}(\mathbf{r}', t') d\mathbf{r}' dt', \quad (19)$$

where  $T$  is the transfer function (or Green function) and the integrals run over the whole system and times  $t' < t$  to preserve causality (equivalently, one can note that any causal  $T$  must be zero for  $t' < t$  and integrate over all  $t'$ ) [126–128,131]. The transfer function contains complete information on the brain’s linear properties, responses, and dynamics, and is equivalent to the total effective connectivity between  $\mathbf{r}$  and  $\mathbf{r}'$  via direct and indirect paths [8,12,49,50,104,130]

Under our assumption of a symmetric operator  $D_r$ ,  $T$  can be written in terms of orthonormal eigenfunctions as [12,49,56,126–128,131]

$$T(\mathbf{r}, \mathbf{r}', \tau) = \sum_j u_j(\mathbf{r}) u_j(\mathbf{r}') \theta_j(\tau), \quad (20)$$

where the temporal responses  $\theta_j(\tau)$  remain to be determined. Notice that the multidimensional spatial dependence of the tensor  $T$  on the left-hand side is simplified to a single sum on the right-hand side once the eigenfunctions have been identified.

The transfer function in Eq. (20) is, by definition, the response of the system at  $\mathbf{r}$  and  $t' + \tau$  to a unit delta-function perturbation at  $\mathbf{r}'$  and  $t'$ , and thus satisfies Eq. (10) with a delta-function on the right-hand side. Substitution of the form of Eq. (20) into Eq. (10), and use of the orthonormality of the eigenfunctions, then yields

$$(D_t + K_j^2) \theta_j(\tau) = \delta(\tau). \quad (21)$$

Hence, by Fourier transforming this result with the convention

$$h(\omega) = \int h(t) e^{i\omega t} dt, \quad (22)$$

$$h(t) = \int h(\omega) e^{-i\omega t} \frac{d\omega}{2\pi}, \quad (23)$$

we find

$$\theta_j(\omega) = \frac{1}{D_t(\omega) + K_j^2}. \quad (24)$$

The function  $\theta_j(\omega)$  must satisfy the reality condition  $\theta_j(-\omega) = \theta_j^*(\omega)$  for  $\theta_j(\tau)$  to be real, where the asterisk denotes the complex conjugate.

### C. Expansion in modal resonances

Generally, transfer functions have a very complicated form owing to the complexities of  $D_t(\omega)$  that arise from local dynamics of multiple neural populations and loops connecting cortex to thalamus, for example. Hence, in engineering control theory it is common to approximate them by rational functions of  $\omega$  or the Laplace-transform equivalent [61,62,65] and such ideas have been used in brain dynamics for decades [124,132]. One thus writes [60]

$$\theta_j(\omega) \approx \frac{\sum_{q=0}^m B_{jq}(-i\omega)^q}{\sum_{p=0}^n A_{jp}(-i\omega)^p}, \quad (25)$$

where  $m < n$  and the  $A_{jp}$  and  $B_{jq}$  are constants. The denominator of Eq. (25) is a polynomial in  $-i\omega$ , so it can be written as a product of  $n$  linear factors, each of which has a zero at a location  $\omega_{jp}$  in the complex plane. If we assume for simplicity that the poles are distinct, then we can then use a rational function decomposition to approximate  $\theta_j(\omega)$ , as a sum over these poles, which gives

$$\theta_j(\omega) \approx \sum_p \frac{r_{jp}}{\omega - \omega_{jp}}, \quad (26)$$

$$= \sum_p \frac{r_{jp}}{\omega - \Omega_{jp} + i\gamma_{jp}} \quad (27)$$

(we omit the explicit bound on sums from now on), where  $r_{jp}$  is a complex constant,  $\omega_{jp} = \Omega_{jp} - i\gamma_{jp}$  is a complex resonant frequency,  $\Omega_{jp}$  is the corresponding frequency of oscillation, and  $\gamma_{jp}$  is the damping rate; both  $\Omega_{jp}$  and  $\gamma_{jp}$  are real and  $\gamma_{jp}$  must be positive for stability. Responses are strongest at modal resonances and Eq. (27) has been found to provide an accurate approximation even for small numbers  $n$  of poles [60].

The poles are divided into two classes. In the first class,  $\Omega_{jp} \neq 0$ , which corresponds to oscillations, so there must be another pole  $p'$  with  $r_{jp'} = -r_{jp}^*$ ,  $\Omega_{jp'} = -\Omega_{jp}$ , and  $\gamma_{jp'} = \gamma_{jp}$ , or else the reality condition would not be satisfied. It is convenient to symmetrize these functions by writing

$$\Theta_{jp}(\omega) = \frac{1}{2}[\theta_{jp}(\omega) + \theta_{jp'}(\omega)], \quad (28)$$

$$= \frac{1}{2} \left[ \frac{r_{jp}}{\omega - \Omega_{jp} + i\gamma_{jp}} - \frac{r_{jp}^*}{\omega + \Omega_{jp} + i\gamma_{jp}} \right], \quad (29)$$

$$= \frac{i(\omega + i\gamma_{jp})\text{Im}(r_{jp}) + \Omega_{jp}\text{Re}(r_{jp})}{(\omega + i\gamma_{jp})^2 - \Omega_{jp}^2}, \quad (30)$$

$$= \frac{\mathcal{D}'_{jp}(\omega)}{\mathcal{D}_{jp}(\omega)}, \quad (31)$$

where  $\mathcal{D}'_{jp}(\omega)$  and  $\mathcal{D}_{jp}(\omega)$  are defined to be the numerator and denominator on the right-hand side of Eq. (30), respectively.

Note that we use upper case  $\Theta$  here to emphasize the symmetrization. In the second class of poles,  $\Omega_{jp} = 0$ ,  $r_{jp}$  is real, and these resonances are purely damped. In this case,

$$\Theta_{jp}(\omega) = \theta_{jp}(\omega). \quad (32)$$

In the above symmetrized notation, one has

$$\theta_j(\omega) = \sum_p \Theta_{jp}(\omega). \quad (33)$$

Depending on the accuracy required, it is possible to systematically truncate this sum to include only the least damped poles, thereby capturing the dominant dynamics in a compact form [61,65,124].

### D. Modal-polar equations of motion

We now express the linear dynamics of Eq. (10) in terms of individual modes and poles. If we substitute the general eigenfunction expansions

$$Q^{(1)}(\mathbf{r}, t) = \sum_j q_j^{(1)}(t) u_j(\mathbf{r}), \quad (34)$$

$$N^{(1)}(\mathbf{r}, t) = \sum_j n_j^{(1)}(t) u_j(\mathbf{r}), \quad (35)$$

into Eq. (10), then the dynamics of  $q_j^{(1)}(t)$  can be analyzed by first writing

$$q_j^{(1)}(t) = \sum_p q_{jp}^{(1)}(t), \quad (36)$$

where each term on the right-hand side represents the symmetrized response of one pole. The dynamics due to individual symmetrized poles are best approached via Fourier space, where one can write the response in pole  $p$  of mode  $j$  to the component of the stimulus in mode  $j$  as

$$q_{jp}^{(1)}(\omega) = \Theta_{jp}(\omega) n_j^{(1)}(\omega), \quad (37)$$

or, equivalently from Eq. (31),

$$\mathcal{D}_{jp}(\omega) q_{jp}^{(1)}(\omega) = \mathcal{D}'_{jp}(\omega) n_j^{(1)}(\omega). \quad (38)$$

Equation (37) can be inverse transformed to the time domain. Noting that a time derivative corresponds to a factor of  $-i\omega$  in Fourier space, this leads to the ordinary differential equation

$$\mathcal{D}_{jp}(t) q_{jp}^{(1)}(t) = \mathcal{D}'_{jp}(t) n_j^{(1)}(t). \quad (39)$$

When  $\Omega_{jp} \neq 0$ ,

$$\mathcal{D}_{jp}(t) = \left( \frac{d}{dt} + \gamma_{jp} \right)^2 + \Omega_{jp}^2, \quad (40)$$

$$\mathcal{D}'_{jp}(t) = \text{Im}(r_{jp}) \left( \frac{d}{dt} + \gamma_{jp} \right) - \text{Re}(r_{jp}) \Omega_{jp}. \quad (41)$$

When  $\Omega_{jp} = 0$ , the corresponding expressions are

$$\mathcal{D}_{jp}(t) = \frac{d}{dt} + \gamma_{jp}, \quad (42)$$

$$\mathcal{D}'_{jp}(t) = -ir_{jp}. \quad (43)$$

The above results express the dynamics of  $q_{jp}^{(1)}$  in terms of  $n_j^{(1)}$  and its time derivative. In particular, Eq. (39) describes

how external inputs drive resonant activity that is “broadcast” across the brain in the corresponding spatial mode  $u_j(\mathbf{r})$ . Arriving at other locations, this activity drives neurons and is thus “read out” through its effects on their dynamics. A coordinate-space version of this picture formed the basis of a hybrid spiking neuron-NFT method proposed to speed large-scale spiking neuron computations [98].

Solutions of Eq. (38) can be summed over  $p$  to obtain  $q_j^{(1)}(t)$  and then the solution of Eq. (10) via Eq. (34). Explicitly,

$$Q^{(1)}(\mathbf{r}, t) = \sum_j u_j(\mathbf{r}) \sum_p q_{jp}^{(1)}(t), \quad (44)$$

From Eqs. (36) and (37) we see that the right-hand side of Eq. (44) depends only on the  $u_j$ ,  $\theta_j$ , and  $n_j^{(1)}(t)$ , in accord with eigenmodes being independent of one another in the linear regime.

The sums in Eq. (44) can be systematically truncated to retain however many of the largest terms are relevant to a given problem, thereby providing a discrete, compact representation. We discuss how to estimate the factors on the right-hand side from data in Sec. VII.

#### IV. NONLINEAR TERMS AND DISCRETE SPECTRAL NETWORK

We now turn to the nonlinear dynamics of Eq. (11), into which we substitute Eq. (34) and the expression

$$Q^{(2)}(\mathbf{r}, t) = \sum_k q_k^{(2)}(t) u_k(\mathbf{r}), \quad (45)$$

such that the solution Eq. (11) can be determined to second order in the perturbation  $N^{(1)}$ . This yields

$$\begin{aligned} (D_t + D_r) \sum_k q_k^{(2)}(t) u_k(\mathbf{r}) \\ = a \sum_{lm} u_l(\mathbf{r}) u_m(\mathbf{r}) q_l^{(1)}(t) q_m^{(1)}(t), \end{aligned} \quad (46)$$

which expresses the dynamics of  $q_k^{(2)}$  in terms of the set of  $q_m^{(1)}$ , thereby establishing a discrete network of interactions.

If we invoke Eq. (14), multiply both sides of Eq. (46) by  $u_j(\mathbf{r})$ , and integrate the result over all  $\mathbf{r}$  to project out the contribution to mode  $j$ , then we find

$$(D_t + K_j^2) q_j^{(2)}(t) = a \sum_{lm} b_{jlm} q_l^{(1)}(t) q_m^{(1)}(t), \quad (47)$$

$$b_{jlm} = \int u_j(\mathbf{r}) u_l(\mathbf{r}) u_m(\mathbf{r}), \quad (48)$$

where the coupling coefficients  $b_{jlm}$  are analogous to the Clebsch-Gordan coefficients from quantum mechanics, and are discussed further below [126,133]. Equation (47) expresses what is termed three-wave coupling in nonlinear plasma theory and nonlinear optics [70,72,134–136]—modes  $l$  and  $m$  couple nonlinearly to drive mode  $j$ , provided  $b_{jlm} \neq 0$ .

The operator on the left-hand side of Eq. (11) is identical to the one on the left-hand side of Eq. (10). Hence, the same

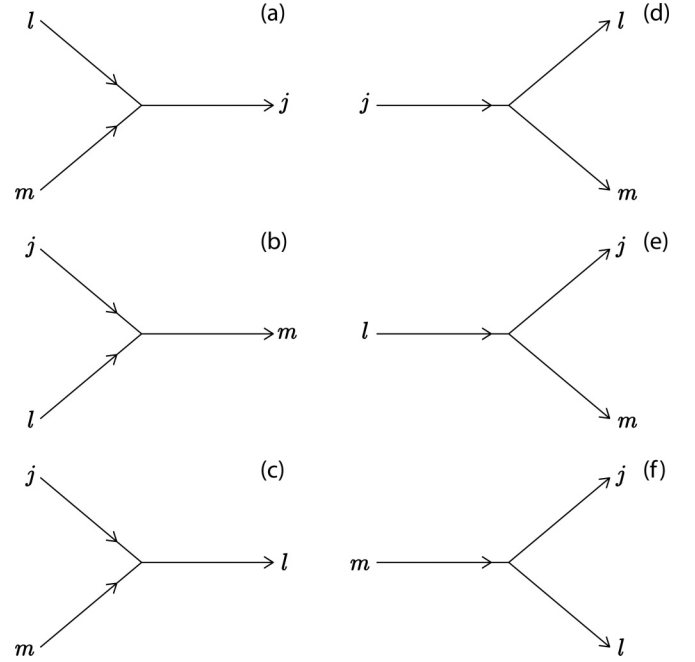


FIG. 1. Three-wave coalescence processes in frames (a–c), and decay processes in frames (d–f), all of which involve the spatial overlap factor  $b_{jlm}$ .

steps as in Sec. III yield the polar expansion

$$\mathcal{D}_{jp}(t) q_{jp}^{(2)}(t) = a \sum_{lm} b_{jlm} \mathcal{D}'_{jp}(t) [q_l^{(1)}(t) q_m^{(1)}(t)], \quad (49)$$

which describes the evolution of the contribution of resonance  $p$  to the second-order part of the amplitude of mode  $j$ . The nonlinear drive in the square brackets on the right-hand side can, of course, be decomposed into polar contributions via Eqs. (36) and (39), thereby delivering a nonlinear coupling equation for the excitation of various modal resonances. Equation (49) governs mode-mode interactions and, along with Eq. (47), is one of the key findings of the present paper.

A number of further aspects of Eq. (49) are worth commenting on:

(i) This formulation neatly separates spatial aspects from temporal ones.

(ii) The spatial overlap integral  $b_{jlm}$  does not depend on the second-order dynamical process involved, but expresses the coefficient of  $u_j(\mathbf{r})$  in the eigenfunction decomposition of the product  $u_l(\mathbf{r}) u_m(\mathbf{r})$  and is symmetric in all its subscripts. It thus arises in any of the three-mode coalescence and decay processes seen in Fig. 1, which are discussed further below and are related by crossing symmetries [137]. Not all such coefficients are nonzero: in 1D or 2D planar geometries, the eigenfunctions are plane waves and this factor is only nonzero if the interaction conserves linear momentum; in the 2D spherical case, the eigenfunctions are spherical harmonics and angular momentum conservation implies that the overlap integral is only nonzero for certain combinations of the three modes involved [126,129,133]; and, in the general case, coefficients where characteristic wave numbers  $K_j$  do not satisfy similar relations will tend to be small for similar reasons.

(iii) The operators  $\mathcal{D}_{jp}$  and  $\mathcal{D}'_{jp}$  do not change the frequencies of the quantities they operate on because they simply become multiplicative factors in Fourier space. Hence, the Fourier transform of Eq. (49) is of the form

$$q_{jp}^{(2)}(\omega) = a\Theta_{jp}(\omega) \sum_{lm} b_{jlm} \int q_l^{(1)}(\omega - \omega') q_m^{(1)}(\omega') \frac{d\omega'}{2\pi}, \quad (50)$$

where we recall Eq. (31). Equation (50) thus describes the three-wave coalescence shown in Fig. 1(a), in which oscillations in modes  $l$  and  $m$  interact to excite mode  $j$ . The variables  $\omega - \omega'$  and  $\omega'$  could equally well be exchanged, which expresses the symmetry between these modes seen in Fig. 1. Both amplitude and phase coupling are included via the complex amplitudes in Eq. (50), thereby providing a systematic way to treat the wide variety of wave-wave interactions mentioned in the Introduction. The structure of this equation implies that nonlinear coalescence will be strongest when the coalescing waves are both on-resonance.

(iv) The reality condition implies that every Fourier component at  $\omega$  is associated with a complex conjugate term at  $-\omega$ . Hence, all the processes illustrated in Fig. 1 are also encompassed by variants of Eq. (49) obtained by permuting the subscripts.

(v) Results of the type seen in Eqs. (49)–(52) are commonly found in nonlinear plasma theory and nonlinear optics. Another perspective is obtained by considering Eq. (50) and noting that resonances select out narrow-band responses on the right-hand side. If we then approximate the two factors of  $q^{(1)}$  on the right-hand side of Eq. (49) as monochromatic sinusoidal waves, then their product contains frequencies only at their sum and difference frequencies, as has been seen in steady-state visual evoked responses in experiment [85] and NFT calculations [86,87].

Polar expansion of the integrand in Eq. (50) yields

$$q_{jp}^{(2)}(\omega) = a\Theta_{jp}(\omega) \sum_{lm} b_{jlm} \sum_{sv} \times \int \frac{r_{ls}}{\omega - \omega' - \Omega_{ls} + i\gamma_{ls}} \frac{r_{mv}}{\omega' - \Omega_{mv} + i\gamma_{mv}} \times n_l^{(1)}(\omega - \omega') n_m^{(1)}(\omega') \frac{d\omega'}{2\pi}, \quad (51)$$

$$= a\Theta_{jp}(\omega) \sum_{lm} b_{jlm} \sum_{sv} \times \frac{-ir_{ls}r_{mv}}{\omega - (\Omega_{ls} + \Omega_{mv}) + i(\gamma_{ls} + \gamma_{mv})} \times n_l^{(1)}(\omega - \Omega_{mv} + i\gamma_{mv}) n_m^{(1)}(\Omega_{mv} + i\gamma_{mv}), \quad (52)$$

where we have obtained Eq. (52) from Eq. (51) via the Cauchy residue theorem after integration along the contour  $C$  in the complex- $\omega'$  plane, shown in Fig. 2, in the limit that the contour radius  $R$  approaches infinity. We see that the quotient on the right-hand side is maximal when the denominator is minimal; i.e., when  $\omega \approx \Omega_{ls} + \Omega_{mv}$ , which is the usual condition for energy conservation in the three-wave coalescence in Fig. 1(a). The average of the right-hand side corresponds to  $\omega = 0$  and is thus maximal in magnitude for  $\Omega_{ls} = -\Omega_{mv}$ .

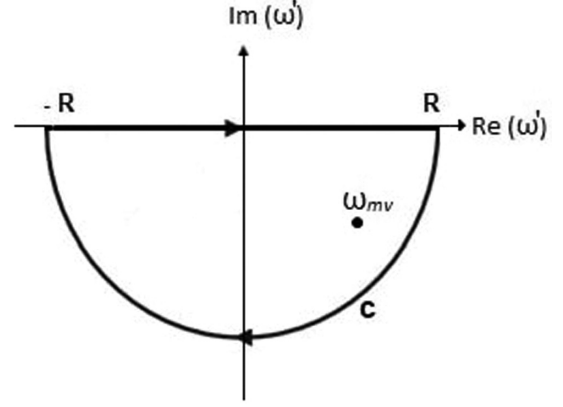


FIG. 2. Contour  $C$  in the complex- $\omega'$  plane used to obtain Eq. (52) from Eq. (51). A pole of the integrand in Eq. (51) at  $\omega_{mv} = \Omega_{mv} - i\gamma_{mv}$  is shown. The limit  $R \rightarrow \infty$  is taken when invoking the Cauchy residue theorem.

In the case of random-phase inputs, which are appropriate for spontaneous activity, the product of  $n^{(1)}$  terms also tends to be large for  $\omega = 0$  or  $\omega = 2\Omega_{mv}$ , which favor rectification and second-harmonic generation, respectively. Second-harmonic generation is also favored by the approximately harmonic relationship between the main corticothalamic resonances predicted theoretically using specific equations analogous to Eq. (1) and observed experimentally in waking states: these are approximately zeroth, first, and second harmonics of the alpha frequency for all the lowest modes [59]. Generation of second harmonics of sleep-spindle waves has also been predicted and observed experimentally [69].

When we consider that every pole is either nonoscillatory or has a partner at an equal and opposite real frequency, we see that there is a network of interactions between these resonances. Figure 3 shows how a spectrum of external inputs  $n^{(1)}$  is resonantly filtered by the system transfer function of the  $j$ th mode  $\theta_j$ . Together the spatially independent eigenfunctions and the strong resonances form a spectral network whose members interact as shown in Fig. 4. By analogy with such interactions in plasmas, one expects energy to interact between scales [134,135]. This may provide a means of systematically communicating information between the short scales of local processing and the long scales of global brain states, and vice versa.

An idea of when nonlinear interactions are likely to become significant can be obtained from known cases in which second harmonic generation and other wave-wave phenomena have been observed. These include generation of the second harmonic of spindle waves [69] and wave-wave interactions in steady-state evoked potential experiments [85,86]. In both cases, the waves involved EEG amplitudes that were considerably higher than most spontaneous EEG signals, but nowhere near the extreme levels seen in epileptic seizures, for example.

## V. SPECTRAL METHODS FOR NUMERICAL SIMULATION OF STRONG NONLINEARITIES

In the linear regime, expansion in eigenfunctions provides a rapid way to evolve activity, because the undriven



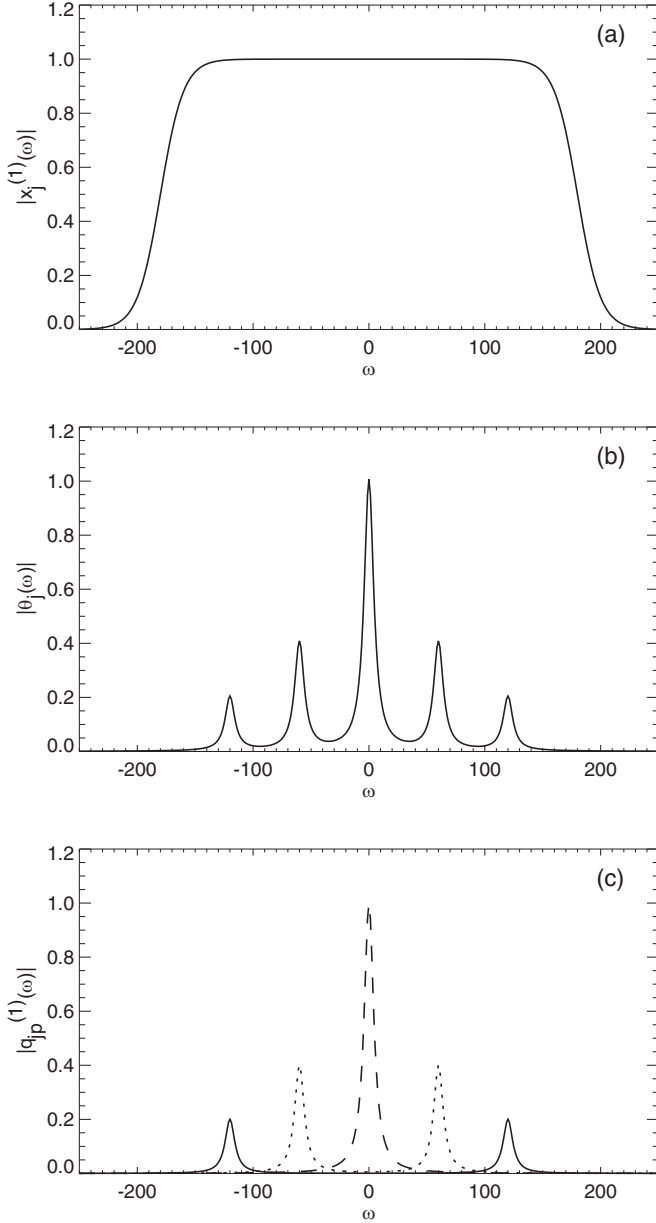


FIG. 3. Schematic resonant dynamics. (a) Magnitude of input signal in mode  $j$ ,  $|n_j^{(1)}(\omega)|$  vs  $\omega$  (in units of  $\text{s}^{-1}$ ), with a white-noise spectrum out to a cutoff frequency  $\omega_c$  much higher than any significant system responses. (b) Magnitude of the temporal transfer function  $|\theta_j(\omega)|$  for mode  $j$ . (c) Resulting polar contributions  $|q_{jp}^{(1)}(\omega)|$ , distinguished by line styles, with pairs indicated by the same style.

mode evolution is exactly known, and driving can easily be added [45,54,59]. It is possible to use modes to expand strong nonlinear interactions to higher order in the perturbations than above, but this rapidly becomes prohibitively complicated. Numerical analysis is thus demanded, but fine simulations of large systems can still be slow. Here we draw on methods from nonlinear plasma physics to show how nonlinear terms can be incorporated into a hybrid numerical method where linear dynamics is ac-

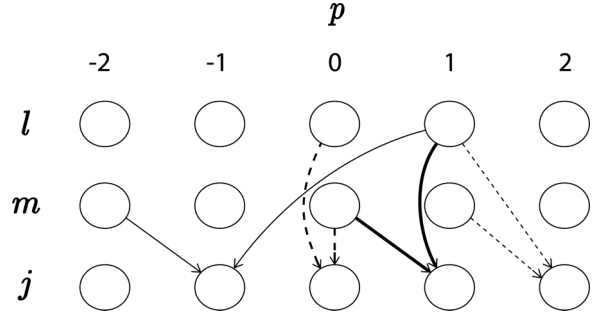


FIG. 4. Schematic of spectral network of three-wave interactions between resonances  $p$  in modes  $lm$  to produce mode  $j$ . These correspond to the types of interactions seen in Fig. 1. Each modal resonance is indicated by a circle and arrows indicate examples of pairs of modes that coalesce to produce a third, each case distinguished by a different line style. Any of these processes can be reversed to yield a corresponding decay.

counted for exactly and nonlinear terms are treated as drives [138].

The overall activity  $Q(\mathbf{r}, t)$  is a sum of contributions from various modes and poles, so we need only consider a single pole here, labeled  $jp$ . In this case, in the linear regime,

$$q_{jp}^{(1)}(\omega) = \theta_{jp}(\omega)n_j^{(1)}(\omega), \quad (53)$$

$$= \frac{r_{jp}}{\omega - \Omega_{jp} + i\gamma_{jp}} n_j^{(1)}(\omega), \quad (54)$$

where we use the unsymmetrized form of  $\theta_{jp}(\omega)$  because we are only dealing with one pole.

If we multiply both sides of Eq. (54) by  $-i$  times the denominator on the right-hand side and inverse Fourier transform the result, then we find

$$\left[ \frac{d}{dt} + i\Omega_{jp} + \gamma_{jp} \right] q_{jp}^{(1)}(t) = -ir_{jp}n_j^{(1)}(t). \quad (55)$$

We now make the ansatz that

$$q_{jp}^{(1)}(t) = a_{jp}(t) \exp[-i\Omega_{jp}t - \gamma_{jp}t], \quad (56)$$

where  $a_{jp}(t)$  is a time-varying amplitude. When the drive vanishes, the form of Eq. (56) is an exact solution of Eq. (55) with constant amplitude  $a_{jp}(t)$ , but the amplitude varies when the drive is activated. More generally, substitution of this ansatz into Eq. (55) yields

$$\frac{da_{jp}(t)}{dt} = -ir_{jp}n_j^{(1)}(t) \exp[i\Omega_{jp}t + \gamma_{jp}t]. \quad (57)$$

The need to avoid overflow due to the exponential of  $\gamma_{jp}t$  limits use of this form to short time intervals, but this suffices for an individual timestep in a numerical integration scheme [138].

Nonlinear effects, even if strong, can now be incorporated by treating them as an additional drive via the expansion

$$Z(\mathbf{r}, t) = \sum_j z_j(t)u_j(\mathbf{r}), \quad (58)$$

whence

$$\frac{da_{jp}(t)}{dt} = -ir_{jp}[n_j^{(1)}(t) + z_j(t)] \exp[i\Omega_{jp}t + \gamma_{jp}t]. \quad (59)$$

At each timestep,  $Z(\mathbf{r}, t)$  is evaluated by first computing  $Q(\mathbf{r}, t)$  by summing  $q_{jp}(t)u_j(\mathbf{r})$  over modes and poles. The result is substituted into whatever functional form is being used for  $Z(\mathbf{r}, t)$ , then Eq. (18) is used to find  $z_j(t)$ . In doing this, we omit the superscript (1) on  $q_{jp}(t)$  because the amplitude now includes nonlinear effects.

In nonlinear plasma physics, the above procedure has been found to vastly speed up nonlinear simulations because the linear dynamics are exactly known and only the nonlinear effects and external drives need be tracked by detailed integration each timestep [138]. Typically, even in strongly nonlinear regimes, only a few timesteps per linear oscillation are required, instead of using multiple steps to integrate oscillatory dynamics that are already exactly known from linear theory [138]. It is anticipated that similar improvements will be achievable for neural field simulations, but their extent will depend on the precise equations being solved. An additional advantage is that the role of modes and poles is explicit in this formulation.

## VI. DIAGNOSTICS FROM MODAL-POLAR ANALYSIS

Having exhibited a compact representation of linear and nonlinear activity and interactions, we examine some quantities such as the bispectrum that can be used to detect mode-mode interactions and others for which we can exploit the modal-polar formulation to derive compact expressions. Correlations between activity at different points in coordinate space are widely used to define two-point functional connectivity on the assumption that correlated activity implies common involvement in brain function and we show how to write these in modal-polar form [6,139]. Our above analysis of the dynamics of Eq. (1) and how it gives rise to activity patterns via spatially extended eigenmodes and resonances also suggests other measures. Additionally, we show how to express the power spectrum and spectral entropy in compact form—both quantities that are widely used in applications.

### A. Bispectrum

The insights obtained via the three-wave analysis in Sec. IV enable us to propose diagnostics for such nonlinearities. We can write Eq. (52) in the form

$$q_{jp}^{(2)}(\omega) = a\Theta_{jp}(\omega) \sum_{lm} b_{jlm} \sum_{sv} a_{lsmv}(\omega), \quad (60)$$

where comparison of Eqs. (52) and (60) defines  $a_{lsmv}(\omega)$ . Here the overlap integral  $b_{jlm}$  governs coupling between spatial eigenmodes, while  $a_{lsmv}(\omega)$  expresses coupling between resonances. Both these factors can be calculated once eigenmodes and their resonant frequencies have been estimated, issues that we discuss in Sec. VII.

Three-wave processes are widely quantified by calculating the bispectrum [22,71,82,140,141]. In our case, the relevant form involves the product

$$B_{jlm}(\omega_1 + \omega_2, \omega_1, \omega_2) = y_j^*(\omega_1 + \omega_2)y_l(\omega_1)y_m(\omega_2), \quad (61)$$

where  $y_j = q_j^{(1)} + q_j^{(2)}$ . This expression must be averaged over multiple time intervals to separate systematically correlated terms from random ones. Note that, because of the separation

of spatial and temporal aspects in the foregoing analysis, it suffices to consider modal amplitudes here and temporarily omit spatial factors.

The lowest-order term in an expansion of Eq. (61) in  $n^{(1)}$  contain products of three first-order terms. These can be significant in coherently driven systems, or during impulse responses, but average to zero under spontaneous conditions if the drives to different modes have random relative phases. The next terms have two factors of  $q_j^{(1)}$  and one of  $q_j^{(2)}$ . Hence, Eq. (52) implies that this contribution involves the coalescence of two waves to produce a third, where one of the two coalescing waves is itself the result of coalescence. (More generally,  $B_{jlm}$  will also involve waves that interact via decays.) In this case, the average of  $B_{jlm}$  over multiple epochs will be nonzero when the waves involved satisfy energy conservation and the pairwise averages of the drives are nonzero; e.g., in the case of random-phase drive, one finds

$$\langle n_j^{(1)}(\omega)n_k^{(1)}(-\omega) \rangle = |n_j^{(1)}(\omega)|^2 \delta_{jk}, \quad (62)$$

where  $|n_j^{(1)}|^2$  is the power spectrum of the drive to mode  $j$  and the angle brackets indicate an average over instances of phase, or over time if ergodic.

The approximation of white noise inputs [i.e.,  $|n_j^{(1)}(\omega)| = \text{constant}$ ] has been found to reproduce a wide range of experimental results on EEG and fMRI phenomena, including spectra of spontaneous EEG activity in waking and sleep states over nearly three decades in frequency, a finding that has been tested in large cohorts of subjects using an NFT that lies within the class described by Eq. (1) [29,30,142,143].

### B. Correlation and covariance

As mentioned above, the two-point correlation function in coordinate space is a common way to quantify functional connectivity in the literature [11], with

$$C(\mathbf{r}, \mathbf{r}', \tau) = \int [Q(\mathbf{r}, t + \tau) - Q^{(0)}(\mathbf{r})] \times [Q(\mathbf{r}', t) - Q^{(0)}(\mathbf{r}', t)] dt, \quad (63)$$

where the integral over  $t$  selects the zero-frequency Fourier component (i.e., the average). The value at  $\tau = 0$  is the covariance, which is the most common method used in the literature to define functional connectivity.

Expansion in eigenfunctions and application of the Wiener-Khintchine theorem [144] then yields

$$C(\mathbf{r}, \mathbf{r}', \tau) = \sum_{jl} u_j(\mathbf{r})u_l(\mathbf{r}') \int e^{-i\omega\tau} q_j^{(1)}(\omega)q_l^{(1)}(-\omega) \frac{d\omega}{2\pi}, \quad (64)$$

to leading order in the perturbation. Hence,

$$C(\mathbf{r}, \mathbf{r}', \tau) = \sum_{jl} u_j(\mathbf{r})u_l(\mathbf{r}') \times \int e^{-i\omega\tau} \theta_j(\omega)\theta_l(-\omega)n_j^{(1)}(\omega)n_l^{(1)}(-\omega) \frac{d\omega}{2\pi}. \quad (65)$$

In the random-phase limit, we obtain the form

$$C(\mathbf{r}, \mathbf{r}', \tau) = \sum_j u_j(\mathbf{r}) u_j(\mathbf{r}') \times \int e^{-i\omega\tau} |\theta_j(\omega)|^2 |n_j^{(1)}(\omega)|^2 \frac{d\omega}{2\pi}, \quad (66)$$

which is diagonal in the mode number [i.e., the sum over  $l$  has been done via the Kronecker delta in Eq. (62)]. Notably, the leading terms in the correlation function involve only pairs of first-order perturbations, so  $B_{jlm}$  is better suited to detection of three-wave interactions.

Polar expansion allows the integral in Eq. (66) to be expressed as a sum. Following similar steps to those used to obtain Eq. (52) we find

$$C(\mathbf{r}, \mathbf{r}', \tau) \approx \sum_j u_j(\mathbf{r}) u_j(\mathbf{r}') \sum_{sp} \frac{-ir_{jp} r_{js}^* |n_j^{(1)}(\Omega_{jp})|^2}{\Omega_{jp} - \Omega_{js} - i(\gamma_{jp} + \gamma_{js})} \times \exp[-\gamma_{jp}\tau - i\Omega_{jp}\tau]. \quad (67)$$

This result is dominated by the most weakly damped resonances with  $s = p$ , which have the strongest and longest-lived responses [43].

### C. Mode amplitudes

The mode amplitudes  $q_j(t)$  can be obtained via Eq. (18) once the eigenfunctions are known. Unlike the measures in the previous two subsections, this involves no time integration or windowing. Hence, mode amplitudes are well suited to tracking transient dynamics such as evoked responses, but can also be Fourier transformed to calculate correlations of amplitudes and/or phases, or the bispectrum, if desired.

The above points largely obviate the need to work directly in coordinate space, although the resulting spatial quantities can be obtained simply by associating the relevant eigenmodes  $u_j(\mathbf{r})$  with the amplitudes  $q_j(t)$ , just as for the spatial patterns of a violin string.

### D. Power spectrum and total power

The power spectrum in the mode  $j$  is

$$P_j(\omega) = |\theta_j(\omega) n_j^{(1)}(\omega)|^2. \quad (68)$$

If the stimuli to different modes are uncorrelated on average so that Eq. (62) applies, then the total power spectrum is

$$P(\omega) = \sum_j P_j(\omega). \quad (69)$$

We can also calculate the total power to be

$$P_{\text{tot}} = \sum_j \int |\theta_j(\omega)|^2 |n_j^{(1)}(\omega)|^2 \frac{d\omega}{2\pi}, \quad (70)$$

$$\approx \sum_{jp} \int \frac{|r_{jp}|^2 |n_j^{(1)}(\omega)|^2}{(\omega - \Omega_{jp})^2 + \gamma_{jp}^2} \frac{d\omega}{2\pi}. \quad (71)$$

If we change variable to  $z = (\omega - \Omega_{jp})/\gamma_{jp}$ , then we find

$$P_{\text{tot}} = \sum_{jp} \frac{|r_{jp}|^2 |n_j^{(1)}(\Omega_{jp})|^2}{\gamma_{jp}} \int \frac{1}{1+z^2} \frac{dz}{2\pi}, \quad (72)$$

$$= \sum_{jp} \frac{|r_{jp}|^2 |n_j^{(1)}(\Omega_{jp})|^2}{2\gamma_{jp}}, \quad (73)$$

$$= \sum_{jp} P_{jp}, \quad (74)$$

where comparison of Eqs. (73) and (74) defines  $P_{jp}$ , which is the power in the  $p$ th resonance of the  $j$ th mode.

### E. Spectral entropy

Spectral entropy can be used to quantify the complexity of brain activity and has thus been widely proposed as the basis for various measures of consciousness [145–148].

The power spectrum of a temporal signal  $P(\omega)$ , where  $\omega$  is the angular frequency, can be used to define a purely temporal spectral entropy  $S$  as

$$S = - \int P(\omega) \ln \left[ \frac{P(\omega) \Delta\omega}{P_{\text{tot}}} \right] \frac{d\omega}{2\pi}, \quad (75)$$

where an effective bandwidth  $\Delta\omega$  is included to make the argument of the logarithm dimensionless, and is discussed below in the spatiotemporal case. Here,  $P_{\text{tot}}$  is defined by the analog of Eq. (70) without the modal sum. The more complex the signal, the more structure there is in the spectrum, and the larger the entropy, thereby underpinning a number of proposed measures of consciousness [145–148]. Note that  $S$  is defined without dividing by  $P_{\text{tot}}$  in the leading factor on the right-hand side, so that  $S \rightarrow 0$  if  $P(\omega) \rightarrow 0$  as in brain death.

Brain activity varies in both space and time and its spectral transform is of the form

$$S = - \sum_j \int P_j(\omega) \ln \left[ \frac{P_j(\omega) \Delta\omega_{jp}}{P_{\text{tot}}} \right] \frac{d\omega}{2\pi}, \quad (76)$$

where  $\Delta\omega_{jp}$  is an effective bandwidth and

$$P_j(\omega) = \sum_p |\theta_{jp}(\omega)|^2 |n_j^{(1)}(\omega)|^2, \quad (77)$$

from Eqs. (33) and (68).

By substituting Eq. (26) into Eq. (77) we thus find

$$S = - \sum_j \int \left[ \sum_{pq} \frac{r_{jp}}{\omega - \omega_{jp}} \frac{r_{jq}^*}{\omega - \omega_{jq}^*} |n_j^{(1)}(\omega)|^2 \right] \times \ln \left[ \frac{\Delta\omega_{jp}}{P_{\text{tot}}} \sum_{lm} \frac{r_{jl}}{\omega - \omega_{jl}} \frac{r_{jm}^*}{\omega - \omega_{jm}^*} |n_j^{(1)}(\omega)|^2 \right] \frac{d\omega}{2\pi}, \quad (78)$$

$$= - \sum_j \int \left[ \sum_{pq} \frac{r_{jp} r_{jq}^* |n_j^{(1)}(\omega)|^2}{(\omega - \Omega_{jp} + i\gamma_{jp})(\omega - \Omega_{jq} - i\gamma_{jq})} \right] \times \ln \left[ \frac{\Delta\omega_{jp}}{P_{\text{tot}}} \sum_{lm} \frac{r_{jl} r_{jm}^* |n_j^{(1)}(\omega)|^2}{(\omega - \Omega_{jl} + i\gamma_{jl})(\omega - \Omega_{jm} + i\gamma_{jm})} \right] \times \frac{d\omega}{2\pi}. \quad (79)$$

The terms in the sums in Eq. (79) are largest in magnitude when the denominators are smallest. This occurs when  $\omega = \Omega_{jp}$  or  $\omega = \Omega_{jq}$  and the largest terms of all occur when both these conditions are satisfied, which selects  $p = q$  in the leading factor and, similarly  $l = m = p$  in the argument of the logarithm. Then

$$S \approx - \sum_{jp} \int \frac{|r_{jp}|^2 |n_j^{(1)}(\omega)|^2}{(\omega - \Omega_{jp})^2 + \gamma_{jp}^2} \times \ln \left[ \frac{\Delta\omega_{jp}}{P_{\text{tot}}} \frac{|r_{jp}|^2 |n_j^{(1)}(\omega)|^2}{(\omega - \Omega_{jp})^2 + \gamma_{jp}^2} \right] \frac{d\omega}{2\pi}. \quad (80)$$

We evaluate the integral in Eq. (80) by dividing numerator and denominator by  $\gamma_{jp}^2$  and changing variables to  $z = (\omega - \Omega_{jp})/\gamma_{jp}$ . This yields

$$S \approx - \sum_{jp} \frac{|r_{jp}|^2 |n_j^{(1)}(\omega)|^2}{\gamma_{jp}} \int \frac{1}{1+z^2} \times \left[ \ln \left( \frac{\Delta\omega_{jp} |r_{jp}|^2 |n_j^{(1)}(\omega)|^2}{P_{\text{tot}} \gamma_{jp}^2} \right) - \ln(1+z^2) \right] \frac{dz}{2\pi}, \quad (81)$$

$$\approx - \sum_{jp} \frac{|r_{jp}|^2 |n_j^{(1)}(\Omega_{jp})|^2}{2\gamma_{jp}} \ln \left[ \frac{\Delta\omega_{jp} |r_{jp}|^2 |n_j^{(1)}(\Omega_{jp})|^2}{4P_{\text{tot}} \gamma_{jp}^2} \right]. \quad (82)$$

$$= - \sum_{jp} P_{jp} \ln \left[ \frac{P_{jp} \Delta\omega_{jp}}{2\gamma_{jp} P_{\text{tot}}} \right], \quad (83)$$

where we have used Eqs. (73) and (74) in finding the final form.

We can now determine the value of  $\Delta\omega_{jp}$  by considering a case in which all the power is in one modal resonance (which must have  $\Omega_{jp} = 0$  to satisfy the reality condition). In this case,

$$S = -P_{\text{tot}} \ln(\Delta\omega_{jp}/2\gamma_{jp}). \quad (84)$$

In this case, there is minimal disorder, so the entropy should be zero. Hence, we set

$$\Delta\omega_{jp} = 2\gamma_{jp}, \quad (85)$$

whence Eq. (83) becomes

$$S = - \sum_{jp} P_{jp} \ln(P_{jp}/P_{\text{tot}}). \quad (86)$$

Thus, subject to the approximations made above, the modal resonances act as separate states in determining the spatiotemporal spectral entropy, but noting that states with nonzero  $\Omega_{jp}$  must come in pairs.

As noted above,  $S \rightarrow 0$  in cases where  $P_{\text{tot}} \rightarrow 0$  or where all the power is concentrated in a single modal resonance. When the power is spread equally over  $M$  modal resonances,

$$S = P_{\text{tot}} \ln M. \quad (87)$$

An immediate consequence is that  $S$  is greater for a pair of poles with nonzero  $\Omega_{jp}$  than for a single pole, reflecting the

case that the latter is a simple, damped state, whereas the former is oscillating with an extra degree of freedom.

## VII. DETERMINATION OF EIGENFUNCTIONS AND RESONANCES FROM DATA

The results in preceding sections have shown that one can obtain compact representations of brain dynamics in terms of a discrete spectral network of modes and poles. But one would also like to be able to determine these from data without assuming particular dynamic equations *a priori*, although it is also possible to specify a NFT and fit its parameters to reproduce the experimentally inferred modal resonances. Here we briefly outline ways in which eigenmodes and their modal decomposition can be calculated from data. This synthesizes work done elsewhere to establish proof-of-principle, but the references cited below have noted that more needs to be done to refine and validate the experimental data processing pipelines that are involved to minimize noise and artifact. Although this remains an active area of investigation, experimental limitations will likely be overcome in due course and they in no way negate the physical existence of modes, resonances, and the resulting spectral network. The purpose of the present section is to show how the relevant quantities can be determined, in principle, not to resolve the experimental issues involved in doing so. We refer in detail below to Fig. 5, which summarizes the main steps, more details of which can be found in the references cited.

### A. Eigenfunctions

We have seen above that the eigenfunctions  $u_j(\mathbf{r})$  are the same for the activity, transfer function, correlation function, and covariance. Of these, the covariance is easiest to determine by averaging equal-time ( $\tau = 0$ ) spontaneous EEG, magnetoencephalographic (MEG), or fMRI measurements over a period of time, but correlations can also be measured using EEG or MEG, which are sufficiently fast to resolve time delays  $\tau$ . If the covariance is finely discretized in coordinate space, then it can be approximately written in matrix form, with rows and columns indexed by position, and integrals becoming sums. It is essential to discretize finely enough to resolve all the physical features that affect the dynamics, to satisfy the Courant condition if wavelike dynamics are involved [127], and to verify that the results are not sensitive to the discretization chosen—use of nodes from a published discrete structural connectome will not suffice in general.

The eigenvectors of the covariance matrix can be obtained by eigenfunction decomposition [8,12,49,50,55,56,127]. These results can then be interpreted as finely discretized approximations to the continuous eigenfunctions of the original system, including any hidden dynamics that is at scales, or in structures, that are not observed directly. Critically, one must not treat the spatial discretization as being in any way fundamental, or forming an actual brain network. On the contrary, only those features that do not depend on the discretization or thresholding can possibly be properties of the brain itself.

Modeling of specific cases of corticothalamic dynamics can also yield approximate eigenfunctions. For example,



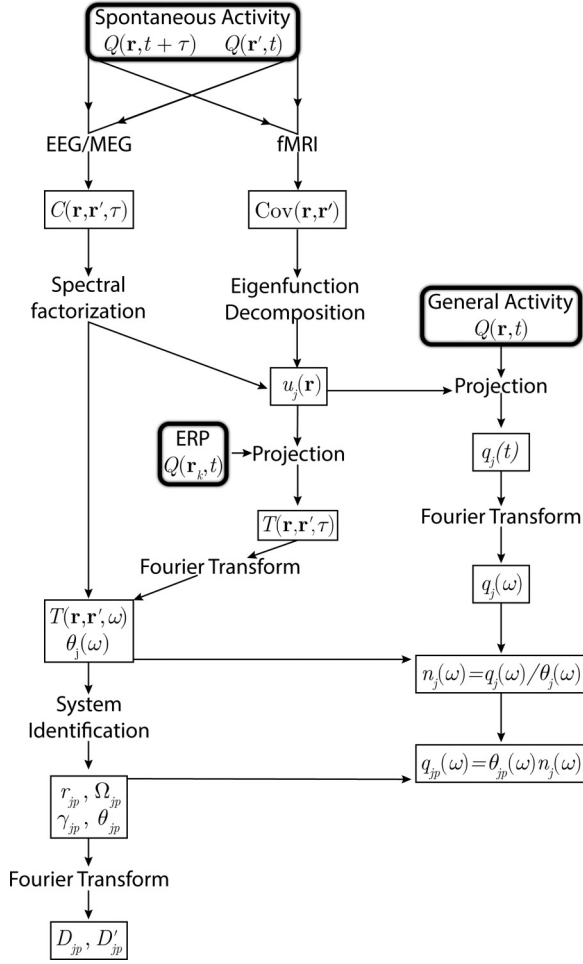


FIG. 5. Schematic of steps involved in estimating eigenfunctions, transfer functions, resonant frequencies, dynamic equations, and mode amplitudes from data. Input data are indicated in car-touches, and results in solid rectangles, linked by the indicated processing steps. Detailed discussion is found in the text.

solution of the Helmholtz equation [which is obtained by setting  $D_r = \nabla^2$  in Eq. (14)] on the cortical surface has been used to obtain approximate eigenfunctions within neural field theory. These prove to be very similar to those found from the covariance and from structural connectivity [50] because the Green function of the resulting NFT equation is very close in form to the distribution of ranges of cortical white matter axons [1,109].

As mentioned in Sec. III A, a number of authors have spectrally factorized statistical covariance matrices to express them compactly in terms of eigenvectors. However, in those cases, these eigenvectors have not been related to the continuous eigenmodes of the underlying dynamics. Eigenvectors have also been widely used as spatial patterns in statistical approaches such as independent component analysis to obtain compact representations of time series, again without relation to dynamics [38]. We reiterate that dynamical eigenmodes and their resonances are privileged over statistical and phenomenological patterns by being fundamental dynamic entities of the brain at macroscopic scales, which means that

they exist independently of investigator choices and data analysis methods.

## B. Transfer function

It has been established that the diagonal form Eq. (59) of the correlation function of background activity can be spectrally factorized in Fourier space to yield the transfer function, so long as relevant time delays are resolved by the measurements [8,56,149–152]; this procedure yields the eigenfunctions and their eigenvalues as byproducts, as summarized in Fig. 5. Alternatively, if the measurements are too slow to resolve the temporal structure of the correlation function, then the spatial covariance can still be spectrally factorized to yield the  $u_j(\mathbf{r})$  and their corresponding eigenvalues.

Once one has estimated the  $u_j(\mathbf{r})$ , one can exploit the fact that the transfer function is by definition the evoked response at a measurement point  $\mathbf{r}$  to a  $\delta$ -function stimulus at a stimulated point  $\mathbf{r}'$  [45,123,131]. Hence, in Eq. (20) we find [12,45]

$$\theta_j(t) = \frac{1}{u_j(\mathbf{r}')} \int T(\mathbf{r}, \mathbf{r}', t) u_j(\mathbf{r}) d\mathbf{r}. \quad (88)$$

All modes are excited by an impulse at  $\mathbf{r}'$  except those that are zero at that point, just as plucking a violin string excites a spectrum of modes, not a pure tone. Evoked responses are routinely measured in electrophysiological studies of cognitive processes [58,153].

Eigenmode methods allow us to efficiently approximate the integral in Eq. (88) if we restrict attention to a finite truncation to the lowest  $L$  modes, choose a stimulus point  $\mathbf{r}'$  and measurement points  $\mathbf{r}_k$  with  $k = 1, \dots, L$ . If the modes are known from the analysis above, then a  $\delta$ -function stimulus at  $\mathbf{r}'$  evokes responses  $Q(\mathbf{r}_k, t)$  at the  $\mathbf{r}_k$ , which can be measured using a fast method such as EEG. If these are in the linear regime, then we can write

$$Q(\mathbf{r}_k, t) = T(\mathbf{r}_k, \mathbf{r}', t), \quad (89)$$

$$\approx \sum_{j=1}^L b_{kj} \theta_j(t), \quad (90)$$

$$b_{kj} = u_j(\mathbf{r}_k) u_j(\mathbf{r}'). \quad (91)$$

As noted in Refs. [12,56], Eq. (90) and its solution can be written in matrix form as

$$Q(t) = B \tilde{\Theta}(t), \quad (92)$$

$$\tilde{\Theta}(t) = B^{-1} Q(t), \quad (93)$$

where  $Q(t)$  and  $\tilde{\Theta}(t)$  [not to be confused with  $\Theta_{jp}(\omega)$  in Eq. (32)] are  $L$ -element column vectors of  $Q(\mathbf{r}_k, t)$  and  $\theta_j(t)$  and the elements of the  $L \times L$  matrix  $B$  are the  $b_{kj}$ . The resulting  $\theta_j(t)$  can then be substituted into Eq. (20) to obtain the transfer function, as shown in Fig. 5. Because only  $L$  observation points are required, spatially coarse-grained methods such as EEG or MEG can be used to determine these temporal aspects of spatially fine-grained modes determined by fMRI.

### C. Estimation of poles

Once one has modal time series  $\theta_j(t)$ , standard methods of system identification from control theory can be used to calculate the polar expansion in Eq. (26) for each mode [61–64]. This involves fitting the dynamics implied by the expansion to the observed time series (e.g., of an evoked response) to estimate the  $r_{jp}$  and  $\omega_{jp}$ , as indicated in Fig. 5. This usually yields a polar expansion in Laplace space, which can be re-expressed in Fourier form. It has also been pointed out that this feature plausibly explains why approaches such as low-dimensional dynamic causal modeling can capture many features of dynamics [48,139,154]. Likewise, coarse-grained approaches may capture the dynamics of the dominant low-order modes through optimization without invoking the modes directly; this may lie at the root of the success of such approaches in some contexts [48,155–157].

As noted in Sec. VIC, it is often useful to have a compact representation of general (i.e., arbitrary) brain activity to simplify interpretation and comparison with theoretical predictions. In this case, one can use the  $u_j(\mathbf{r})$  to compute the relevant coefficients as functions of time by replacing  $g(\mathbf{r})$  by  $Q(\mathbf{r}, t)$  in Eq. (18). The integral can be performed using only a few points by means of the same methods as in Sec. VII B and is indicated by the column headed “General Activity” on the right-hand side of Fig. 5, with the above ERP expansion being one particular case.

## VIII. SUMMARY AND DISCUSSION

This paper has demonstrated how to express brain dynamics and functional connectivity in terms of their intrinsic spatial eigenfunctions and frequency resonances, without relying on the phenomenological and statistical patterns and analyses that are extensively used in the literature. By adopting approaches from neural field theory (NFT), nonlinear physics, and control-systems engineering, this achieves the long-sought goal of a compact, discrete representation of macroscale dynamics and functional connectivity that complements descriptions of local neural activity in coordinate space.

The main results are:

(i) A broad class of macroscopic brain dynamics, embodied in Eq. (1), has been analyzed via a perturbation expansion in orders of input from external stimuli. These equations are sufficiently general to include most types used in NFTs of brain dynamics and connectivity and provide a bridge between NFT and experimental observations of patterns and resonances. Moreover, they do so in a way that relates directly to causal mechanisms.

(ii) Linear terms in the above expansion yield the system transfer function and its discrete expansion in terms of eigenmodes and their frequency resonances, by means of spectral decomposition and control-systems techniques. Eigenmode discreteness arises from boundary conditions on the finite brain, whereas resonances arise chiefly from local dynamics. Systematic truncation of the resulting series of terms is possible, retaining leading terms that dominate the dynamics.

Of all possible spatial patterns, eigenmodes that arise from dynamics are fundamental to the system and thus privileged

over statistical and phenomenological constructs that are common in the literature. Moreover, their analysis can proceed via standard methods, rather than ones that assume the reality of artificially decimated “networks” or graphs that depend on discretization, thresholding, and other investigator-dependent choices.

(iii) Each mode can have multiple resonances and each modal resonance gives rise to an ordinary differential equation for its dynamics in the time domain, as in Eq. (39).

(iv) Second-order terms in the perturbation expansion give rise to three-wave interactions between modal resonances that correspond to coalescences and decays, as in other branches of physics. These couple the linearly independent eigenmodes into a discrete network of interacting entities, allowing transfer of activity between scales. The modal-polar representation allows frequency convolutions that arise in the analysis to be evaluated analytically, as in Eq. (52). Spatial interactions are governed by integrals over products of three eigenmodes that are analogous to Clebsch-Gordan coefficients in quantum theory.

This formulation provides the tools required to quantitatively address wave-wave interactions, amplitude and phase correlations, and other phenomena that are widely observed in the brain (see Introduction). Likewise, they are appropriate to analyze situations pertaining to the communication through coherence (CTC) hypothesis, in which it was argued that in-phase oscillations can facilitate communication between distant neurons [94]. This hypothesis was originally advanced for firing of individual neurons at the microscale, but the present work shows that analogous population-level effects may enhance firing at the macroscale through activity correlated via oscillations in eigenmodes; close correlations between intracellular firing, local field potentials, and EEG recordings have long been established, spanning a wide range of spatial scales [158].

(v) Together with the above results, spectral methods from nonlinear plasma theory open the possibility of fast simulations of even strong nonlinearities by separating linear from nonlinear terms and treating the latter as driving the linear part of the system, whose dynamics are known. This extends the utility of eigenmode analysis from the linear to the nonlinear regime of brain dynamics, which covers strongly driven cases and epileptic seizures, for example.

(vi) Potential diagnostics of functional interactions and connectivity were discussed in the framework of modal-polar interactions. The bispectrum is well suited to detecting three-wave interactions, while correlations and covariances enable calculation of eigenmodes (see below). Spatial modes and their individual resonance amplitudes in the time domain are perhaps the most generally useful quantities, because they do not require the temporal averaging or windowing that is implicit in spectral measures. They can thus be applied to transient phenomena such as evoked responses. The power spectrum and spatiotemporal spectral entropy were also calculated in compact form in terms of modal resonances.

(vii) Because eigenmodes and resonances exist even if the equations governing them are not known, the above results are more general than the specific class of systems embodied in Eq. (1) and analyzed in detail. The results suggest routes by which modal-polar structure can be determined directly

from data by spectral factorization and system-identification methods, as summarized in Fig. 5. Most steps have already been demonstrated in the brain, on synthetic data, and/or in engineering contexts, but some remain to be implemented experimentally in neural systems. It is hoped that the present work will stimulate efforts in this direction by highlighting the utility of obtaining eigenmodes and their resonances in this way.

Turning from the above specific results, it is worth discussing some more general features and implications of the analysis. Most significantly, each mode has a unique spatial structure and each resonance has dynamics that correspond to a data filter that can implement functions such as attention and prediction [65]. Cognitive roles for prominent brain resonances (often called rhythms in the electrophysiological literature) have been speculated upon since their discovery over 90 years ago [57], given significant evidence of long distance correlations in signal-processing pathways [42,58,89]. Notable among theories of this type is the CTC hypothesis mentioned above [94].

When one considers that each mode has its own spatial structure and resonances, plus three-wave interactions with other modes, it is plausible that they serve as spatiotemporal communication channels. In this picture, local neuronal activity would drive eigenmodes of neural fields, which would then influence the firing of distant neurons [98]. Such channels would connect most strongly between spatial antinodes of the modes in question, especially between modes with large spatial coupling as described by the coefficient  $b_{jlm}$  in Eq. (48). The filtering characteristics of resonances would imply that these channels could also carry out information processing tasks such as prediction and attention via gain control [65].

The nonlinear processes that underlie three-wave interactions include the nonlinear firing rate responses that would lead to enhanced neural firing at the peak of each oscillation (especially at spatial antinodes), just as required in CTC and seen in the theta-gamma and other wave-wave interactions mentioned in the Introduction. Thus, the present analysis provides the basis to formulate and test macroscopic versions of CTC and related proposals quantitatively in realistic brain geometries using physiologically based neural field equations. Moreover, analysis of three-wave cascades will illuminate transfer of activity from local processes at small scales up to large scales at which global “broadcast” of relatively few pieces of information to other locations occurs. Such a scenario provides a new perspective on the complementary issues of segregation and integration that may help to illuminate issues relating to consciousness. Notably, the data-filter properties associated with each modal resonance imply that some modal processing of stimuli occurs even during sleep, via spindle and slow-wave resonances. gamma-band resonances in visual cortex may also be relevant in this context.

The results obtained here underline the need to switch between coordinate-space and spectral representations as re-

quired by the problem at hand, just as in quantum physics, where particle and wave representations are each best suited to particular classes of problems. Here, large scale activity and structure are shown to be most easily represented in spectral form. However, localized inputs and readouts of modal activity occur in coordinate space.

The advantages and necessity of a physically based approach via standard mathematical techniques are apparent from the insights obtained above. These approaches allow a shift from phenomenological and statistical analyses to quantitative analysis in terms of causal mechanisms in a framework that unifies and interrelates multiple phenomena. To make greater use of the information contained in data one must thus go beyond patterns and statistics that are based on system decimation via artificial discretizations and thresholding, for example. However, given the widespread use of methods based on graph theory and resting state networks, in particular, one might ask what validity such approaches have, especially given the inability to quantitatively compare results between them [12,19,22,23,34]. Certainly, within a given protocol, it is often possible to reliably detect case-control differences between conditions and subjects, and this can yield useful outcomes. However, it is not possible to make more than qualitative connections to mechanisms and the strong influences of investigator choices (e.g., thresholding, discretization, and processing steps) and resulting artifacts and selection effects must throw such interpretations into significant doubt.

Future directions would usefully include experimental implementation and verification of the steps outlined in Sec. VII for determination of modes and poles directly from data, which would also enable new tests of theoretical models of dynamics. The targets provided for measurement motivate specific improvements in artifact removal and noise reduction in fMRI, EEG, or MEG measurements. Data-driven modes have the advantage that they implicitly incorporate nonuniformities and aspects of dynamics that are not included in models. Application to quantitative analysis of CTC would be highly desirable and would shed light on the relationship between large-scale activity embodied in modes and local signal processing, which is more naturally considered in coordinate space. Other questions that would bear examination would include whether zeros and antinodes of modes coincide with specific functional areas of the brain or their boundaries, or are otherwise related to anatomical structure, as has been suggested for some classes of patterns [35].

## ACKNOWLEDGMENTS

I thank K. M. Aquino and J. A. Henderson for valuable comments on the manuscript and R. El Zghir, D. Naoumenko, and A. Breviario for preparing publication quality versions of figures. This work was supported by the Australian Research Council under Center of Excellence Grant No. CE140100007 and Laureate Fellowship Grant No. FL140100025.

[1] V. Braitenberg and A. Schüz, *Cortex: Statistics and Geometry of Neuronal Connectivity*, 2nd ed. (Springer, Berlin, 1998).

[2] E. R. Kandel, J. H. Schwartz, T. M. Jessell, S. A. Siegelbaum, and A. J. Hudspeth, *Principles of Neural Science*, 5th ed. (McGraw-Hill Education, New York, NY, 2012).

- [3] E. M. Izhikevich and G. E. Edelman, *Proc. Nat. Acad. Sci. USA* **105**, 3593 (2008).
- [4] H. Markram, *Nat. Rev. Neurosci.* **7**, 153 (2006).
- [5] H. Markram, *Cell* **163**, 456 (2015).
- [6] A. Fornito, A. Zalesky, and E. T. Bullmore, *Fundamentals of Brain Network Analysis* (Elsevier, Amsterdam, 2016).
- [7] O. Sporns, *Networks of the Brain* (MIT Press, Cambridge, MA, 2011).
- [8] K. J. Friston, *Human Brain Mapp.* **2**, 56 (1994).
- [9] D. C. Van Essen *et al.*, *NeuroImage* **62**, 2222 (2012).
- [10] S. Arslan, S. I. Ktena, A. Makropoulos, E. C. Robinson, D. Rueckert, and S. Parisot, *NeuroImage* **170**, 5 (2018).
- [11] A. Zalesky, A. Fornito, and E. Bullmore, *NeuroImage* **60**, 2096 (2012).
- [12] P. A. Robinson, *Phys. Rev. E* **99**, 012421 (2019).
- [13] J. W. Scannell, C. Blakemore, and M. P. Young, *J. Neurosci.* **15**, 1463 (1995).
- [14] M. Ercsey-Ravasz, N. T. Markov, C. Lamy, D. C. Van Essen, K. Knoblauch, Z. Toroczkai, and H. Kennedy, *Neuron* **80**, 194 (2013).
- [15] N. T. Markov *et al.*, *Cereb. Cortex* **24**, 17 (2012).
- [16] D. S. Bassett and O. Sporns, *Nat. Neurosci.* **20**, 353 (2017).
- [17] E. Bullmore and O. Sporns, *Nat. Rev. Neurosci.* **10**, 186 (2009).
- [18] S. B. Eickhoff, B. T. T. Yeo, and S. Genon, *Nat. Rev. Neurosci.* **19**, 672 (2018).
- [19] A. Zalesky, A. Fornito, I. H. Harding, L. Cocchi, M. Yücel, C. Pantelis, and E. T. Bullmore, *NeuroImage* **50**, 970 (2010).
- [20] F. C. Yeh, S. Panesar, D. Fernandes, A. Melo, M. Yoshino, J. C. Fernandez-Miranda, J. M. Vettel, and T. Verstynen, *NeuroImage* **178**, 57 (2018).
- [21] A. Schaefer, R. Kong, E. M. Gordon, T. O. Laumann, X. N. Zuo, A. J. Holmes, S. B. Eickhoff, and B. T. T. Yeo, *Cereb. Cortex* **28**, 3095 (2018).
- [22] J. A. Roberts, A. Perry, A. R. Lord, G. Roberts, P. B. Mitchell, R. E. Smith, F. Calamante, and M. Breakspear, *NeuroImage* **124**, 379 (2016).
- [23] J. A. Roberts, A. Perry, G. Roberts, P. B. Mitchell, and M. Breakspear, *NeuroImage* **145**, 118 (2017).
- [24] S. Atasoy, I. Donnelly, and J. Pearson, *Nat. Commun.* **7**, 10340 (2016).
- [25] M. Rubinov and O. Sporns, *NeuroImage* **52**, 1059 (2010).
- [26] E. D. Gireesh and D. Pleniz, *Proc. Nat. Acad. Sci. USA* **105**, 7576 (2008).
- [27] D. Pleniz, *Eur. Phys. J.: Spec. Top.* **205**, 259 (2012).
- [28] P. A. Robinson, *J. R. Soc., Interface* **14**, 20160994 (2017).
- [29] P. A. Robinson, C. J. Rennie, and D. L. Rowe, *Phys. Rev. E* **65**, 041924 (2002).
- [30] P. A. Robinson, C. J. Rennie, D. L. Rowe, and S. C. O'Connor, *Human Brain Mapp.* **23**, 53 (2004).
- [31] E. Salinas and T. J. Sejnowski, *J. Neurosci.* **20**, 6193 (2000).
- [32] E. Salinas and T. J. Sejnowski, *Nat. Rev. Neurosci.* **2**, 539 (2001).
- [33] M. B. Wang, J. P. Owen, P. Mukherjee, and A. Raj, *PLoS Comput. Biol.* **13**, e1005550 (2017).
- [34] H. E. Wang, C. G. Bénar, P. P. Quilichini, K. J. Friston, V. K. Jirsa, and C. Bernard, *Front. Neurosci.* **8**, 405 (2014).
- [35] D. D. Margulies *et al.*, *Proc. Nat. Acad. Sci. USA* **113**, 12574 (2016).
- [36] M. E. Raichle, *Brain Conn.* **1**, 3 (2011).
- [37] B. T. T. Yeo, F. M. Krienen, J. Sepulcre, M. R. Sabuncu, D. Lashkari, M. Hollinshead *et al.*, *J. Neurophysiol.* **106**, 1125 (2011).
- [38] C. F. Beckmann, M. DeLuca, J. T. Devlin, and S. M. Smith, *Philos. Trans. R. Soc. B* **360**, 1001 (2005).
- [39] R. M. Braga, D. J. Sharp, C. Leeson, R. J. S. Wise, and R. Leech, *J. Neurosci.* **33**, 14031 (2013).
- [40] J. S. Damoiseaux, S. A. R. B. Rombouts, F. Barkhof, P. Scheltens, C. J. Stam, S. M. Smith, and C. F. Beckmann, *Proc. Nat. Acad. Sci. USA* **103**, 13848 (2006).
- [41] G. Lioi, V. Gripon, A. Brahim, F. Rousseau, and N. Farrugia, *Network Neurosci.* **5**, 322 (2021).
- [42] P. L. Nunez, *Neocortical Dynamics and Human EEG Rhythms* (Oxford, New York, NY, 1995).
- [43] P. A. Robinson, *J. Theor. Biol.* **222**, 163 (2003).
- [44] P. A. Robinson, P. N. Loxley, S. C. O'Connor, and C. J. Rennie, *Phys. Rev. E* **63**, 041909 (2001).
- [45] P. A. Robinson, J. C. Pagès, N. C. Gabay, T. Babaie, and K. N. Mukta, *Phys. Rev. E* **97**, 042418 (2018).
- [46] P. Tewarie, R. Abeysuriya, Á. Byrne, G. C. O'Neill, S. N. Sotiropoulos, M. J. Brookes, and S. Coombes, *NeuroImage* **186**, 211 (2019).
- [47] X. Gao and P. A. Robinson, *Biol. Cybern.* **114**, 643 (2020).
- [48] P. A. Robinson, *Phys. Rev. E* **88**, 054702 (2013).
- [49] P. A. Robinson, S. Sarkar, G. M. Pandejee, and J. A. Henderson, *Phys. Rev. E* **90**, 012707 (2014).
- [50] P. A. Robinson, X. Zhao, K. M. Aquino, J. D. Griffiths, S. Sarkar, and G. Mehta-Pandejee, *NeuroImage* **142**, 79 (2016).
- [51] K. J. Friston, J. Kahan, A. Razi, K. E. Stephan, and O. Sporns, *NeuroImage* **99**, 533 (2014).
- [52] S. Deslauriers-Gauthier, M. Zucchelli, M. Frigo, and R. Deriche, *Med. Image Anal.* **66**, 101799 (2020).
- [53] A. Raj, C. Cai, X. Xie, E. Palacios, J. Owen, P. Mukherjee, and S. Nagarajan, *Hum. Brain Mapp.* **41**, 2980 (2020).
- [54] K. N. Mukta, P. A. Robinson, J. C. Pagès, N. C. Gabay, and X. Gao, *Phys. Rev. E* **102**, 062303 (2020).
- [55] R. F. Galán, *PLoS One* **3**, e2148 (2008).
- [56] J. A. Henderson, M. Dhamala, and P. A. Robinson, *NeuroImage* **235**, 117989 (2021).
- [57] H. Berger, *Arch. Psychiatr. Nervenkr.* **87**, 527 (1929).
- [58] N. Niedermeyer and F. H. Lopes da Silva (eds.) *Electroencephalography: Basic Principles, Clinical Applications, and Related Fields*, 4th ed. (Williams and Wilkins, Baltimore, MD, 1999).
- [59] N. C. Gabay, T. Babaie-Janvier, and P. A. Robinson, *Phys. Rev. E* **98**, 042413 (2018).
- [60] R. K. El-Zghir, N. C. Gabay, and P. A. Robinson, *Front. Hum. Neurosci.* **15**, 642479 (2021).
- [61] R. F. Stengel, *Optimal Control and Estimation* (Dover, New York, NY, 1994).
- [62] S. J. Schiff, *Neural Control Engineering* (MIT Press, Cambridge, MA, 2011).
- [63] T. Söderström and P. Stoica, *System Identification* (Prentice Hall, New York, NY, 1989).
- [64] E. Walter and L. Pronzato, *Identification of Parametric Models from Experimental Data* (Springer, New York, NY, 1997).



- [65] T. Babaie-Janvier and P. A. Robinson, *Front. Neurosci.* **13**, 1240 (2019).
- [66] C. Koch, *Biophysics of Computation* (Oxford University Press, Oxford, UK, 1999).
- [67] P. A. Robinson and N. Roy, *Phys. Rev. E* **91**, 062719 (2015).
- [68] W. Gerstner and W. Kistler, *Spiking Neuron Models: Single Neurons, Populations, Plasticity* (Cambridge University Press, Cambridge, UK, 2002).
- [69] R. G. Abeysuriya, C. J. Rennie, and P. A. Robinson, *J. Theor. Biol.* **344**, 70 (2014).
- [70] R. W. Boyd, *Nonlinear Optics*, 3rd ed. (Academic, Oxford, UK, 2008).
- [71] V. Kravtchenko-Berejnoi, F. Lefeuve, V. Krasnosel'skikh, and D. Lagoutte, *Signal Proc.* **42**, 291 (1995).
- [72] D. B. Melrose and R. C. McPhedran, *Electromagnetic Processes in Dispersive Media* (Cambridge University Press, Cambridge, UK, 1991), Ch. 26.
- [73] M. Ferdousi, T. Babaie-Janvier, and P. A. Robinson, *J. Theor. Biol.* **500**, 110308 (2020).
- [74] C. J. Stam, J. P. M. Pijn, P. Suffczynski, and F. H. Lopes da Silva, *Clin. Neurophysiol.* **110**, 1801 (1999).
- [75] M. Bekisz and A. Wróbel, *NeuroRep.* **10**, 3589 (1999).
- [76] R. T. Canolty, E. Edwards, S. S. Dalal, M. Soltani, S. S. Nagarajan, H. E. Kirsch, M. S. Berger, N. M. Barbaro, and R. T. Knight, *Science* **313**, 1626 (2006).
- [77] J. Chapeton, R. Haque, J. H. Wittig, S. K. Inati, and K. A. Zaghloul, *Curr. Biol.* **29**, 2801 (2019).
- [78] O. Jensen and A. Mazaheri, *Front. Hum. Neurosci.* **4**, 186 (2010).
- [79] M. Massimini, M. Rosanova, and M. Mariotti, *J. Neurophysiol.* **89**, 1205 (2003).
- [80] P. Quilichini, A. Sirota, and G. Buzsáki, *J. Neurosci.* **30**, 11128 (2010).
- [81] P. Sauseng, W. Klimesch, W. Gruber, M. Doppelmayr, W. Stadler, and M. Schabus, *Neurosci. Lett.* **324**, 121 (2002).
- [82] T. Schanze and R. Eckhorn, *Int. J. Psychophysiol.* **26**, 171 (1997).
- [83] E. Spaak, M. Zeitler, and S. Gielen, *PLoS One* **7**, e45688 (2012).
- [84] J. Igarashi, Y. Isomura, K. Arai, R. Harukuni, and T. Fukai, *J. Neurosci.* **33**, 18515 (2013).
- [85] C. Herrmann, *Exp. Brain Res.* **137**, 346 (2001).
- [86] J. A. Roberts and P. A. Robinson, *NeuroImage* **62**, 1947 (2012).
- [87] M. Ferdousi, T. Babaie-Janvier, and P. A. Robinson, *J. Theor. Biol.* **460**, 184 (2019).
- [88] C. A. Bosman *et al.*, *Neuron* **75**, 875 (2012).
- [89] G. Buzsáki and A. Draguhn, *Science* **304**, 1926 (2004).
- [90] G. Buzsáki and X.-J. Wang, *Ann. Rev. Neurosci.* **35**, 203 (2012).
- [91] R. T. Canolty and R. T. Knight, *Trends Cogn. Sci.* **14**, 506 (2010).
- [92] L. L. Colgin, T. Denninger, M. Fyhn, T. Haftin, T. Bonnevie, O. Jensen, M.-B. Moser, and E. I. Moser, *Nature (London)* **462**, 353 (2009).
- [93] G. Deco and M. L. Kringelbach, *Trends Neurosci.* **39**, 125 (2016).
- [94] P. Fries, *Trends Cogn. Neurosci.* **9**, 474 (2005).
- [95] P. Fries, T. Womelsdorf, R. Oostenveld, and R. Desimone, *J. Neurosci.* **28**, 4823 (2008).
- [96] D. Vidaurre, L. T. Hunt, A. J. Quinn, B. A. E. Hunt, M. J. Brookes, A. C. Nobre, and M. W. Woolrich, *Nat. Commun.* **9**, 2987 (2018).
- [97] S. R. Gohel and B. B. Biswal, *Brain Conn.* **5**, 23 (2015).
- [98] P. A. Robinson and J. W. Kim, Advances in Cognitive Neurodynamics III, in *Proceedings of the 3rd International Conference on Cognitive Neurodynamics*, edited by Y. Yamaguchi (Springer, Dordrecht, 2013), p. 83.
- [99] K. Linkenkaer-Hansen, V. V. Nikulin, S. Palva, R. J. Ilmoniemi, and J. M. Palva, *J. Neurosci.* **24**, 10186 (2004).
- [100] R. Scheeringa, A. Mazaheri, I. Bojak, d. G. Norris, and A. Kleinschmidt, *J. Neurosci.* **31**, 3813 (2011).
- [101] C. E. Schroeder, P. Lakatos, Y. Kajikawa, S. Partan, and A. Puce, *Trends Cogn. Neurosci.* **12**, 106 (2008).
- [102] L. Marzetti, S. Della Penna, A. Z. Snyder, V. Pizzella, G. Nolte, F. de Pasquale, G. L. Romani, and M. Corbetta, *NeuroImage* **79**, 172 (2013).
- [103] P. J. Uhlhaas, G. Pipa, B. Lima, L. Melloni, S. Neuenschwander, D. Nikolić, and W. Singer, *Front. Integ. Neurosci.* **3**, 17 (2009).
- [104] P. A. Robinson, *Phys. Rev. E* **90**, 042712 (2014).
- [105] N. K. Logothetis, J. Pauls, M. Augath, T. Trinath, and A. Oeltermann, *Nature (London)* **412**, 150 (2001).
- [106] S. Coombes, P. beim Graben, R. Potthast, and J. Wright (eds.), *Neural Fields: Theory and Applications* (Springer, Berlin, 2014).
- [107] G. Deco, V. K. Jirsa, P. A. Robinson, M. Breakspear, and K. Friston, *PLoS Comput. Biol.* **4**, e1000092 (2008).
- [108] V. K. Jirsa and H. Haken, *Phys. Rev. Lett.* **77**, 960 (1996).
- [109] P. A. Robinson, C. J. Rennie, and J. J. Wright, *Phys. Rev. E* **56**, 826 (1997).
- [110] M. L. Steyn-Ross, D. A. Steyn-Ross, J. W. Sleight, and D. T. J. Liley, *Phys. Rev. E* **60**, 7299 (1999).
- [111] P. C. Bressloff, *J. Phys. A* **45**, 033001 (2012).
- [112] J. J. Wright and D. T. J. Liley, *Behav. Brain Sci.* **19**, 285 (1996).
- [113] H. R. Wilson and J. D. Cowan, *Biophys. J.* **12**, 1 (1972).
- [114] P. L. Nunez, *Math. Biosci.* **21**, 279 (1974).
- [115] S. Amari, *Biol. Cybern.* **27**, 77 (1977).
- [116] P. L. Nunez and R. Srinivasan, *Clin. Neurophysiol.* **117**, 2424 (2006).
- [117] P. L. Nunez, *Behav. Brain Sci.* **23**, 371 (2000).
- [118] R. L. Beurle, *Philos. Trans. R. Soc. London Ser. B, Biol. Sci.* **240**, 55 (1956).
- [119] F. H. Lopes da Silva, A. Van Rotterdam, P. Barts, E. Van Heusden, and W. Burr, *Prog. Brain Res.* **45**, 281 (1976).
- [120] J. J. Wright and D. T. J. Liley, *Network: Comput. Neural Syst.* **5**, 191 (1994).
- [121] J. J. Wright and D. T. J. Liley, *Biol. Cybern.* **72**, 347 (1995).
- [122] W. J. Freeman, *Biol. Cybern.* **33**, 237 (1979).
- [123] R. Snieder, K. Wapenaar, and U. Wegler, *Phys. Rev. E* **75**, 036103 (2007).
- [124] W. J. Freeman, *Mass Action in the Nervous System* (Academic, New York, NY, 1975).
- [125] P. Jezzard, P. M. Matthews, and S. M. Smith (eds.) *Functional MRI: An Introduction to Methods* (Oxford University Press, Oxford, UK, 2001).
- [126] L. I. Schiff, *Quantum Mechanics*, 3rd ed. (McGraw-Hill Kogakusha, Tokyo, 1968).

- [127] R. Courant and D. Hilbert, *Methods of Mathematical Physics*, 2 vols. (Wiley VCH, Weinheim, 2004).
- [128] P. M. Morse and H. Feshbach, *Methods of Theoretical Physics*, 2 vols. (McGraw-Hill, New York, NY, 1953).
- [129] T. M. Dunster in *NIST Handbook of Mathematical Functions*, edited by F. W. J. Olver, D. W. Lozier, R. F. Boisvert, and C. W. Clark (Cambridge University Press, Cambridge, UK, 2010), Ch. 14.
- [130] P. A. Robinson, *Phys. Rev. E* **85**, 011912 (2012).
- [131] W. Greiner, *Relativistic Quantum Mechanics* (Springer, Berlin, 1990).
- [132] W. J. Freeman, *Ann. Rev. Biophys. Bioeng.* **1**, 225 (1972).
- [133] L. C. Maximon in *NIST Handbook of Mathematical Functions*, edited by F. W. J. Olver, D. W. Lozier, R. F. Boisvert, and C. W. Clark (Cambridge University Press, Cambridge, UK, 2010), Ch. 34.
- [134] P. A. Robinson, *Rev. Mod. Phys.* **69**, 507 (1997).
- [135] V. E. Zakharov, S. L. Musher, and A. M. Rubenchik, *Phys. Rep.* **129**, 285 (1985).
- [136] W. L. Kruer, *The Physics of Laser-Plasma Interactions* (Addison-Wesley, Redwood City, CA, 1988).
- [137] W. Greiner and J. Reinhardt, *Quantum Electrodynamics* (Springer, Berlin, 1994).
- [138] P. A. Robinson and D. L. Newman, *Phys. Fluids B* **1**, 2319 (1989).
- [139] K. J. Friston, B. Li, J. Daunizeau, and K. E. Stephan, *NeuroImage* **56**, 1202 (2011).
- [140] J. Jamšek, A. Stefanovska, P. V. E. McClintock, and I. A. Khovanov, *Phys. Rev. E* **68**, 016201 (2003).
- [141] J. W. Johansen and P. S. Sebel, *Anesthesiol.* **93**, 1336 (2000).
- [142] R. G. Abeysuriya, C. J. Rennie, and P. A. Robinson, *J. Neurosci. Meth.* **253**, 55 (2015).
- [143] S. J. van Albada, C. C. Kerr, A. K. I. Chiang, C. J. Rennie, and P. A. Robinson, *Clin. Neurophysiol.* **121**, 21 (2010).
- [144] F. Reif, *Fundamentals of Statistical and Thermal Physics* (McGraw-Hill, New York, NY, 1965).
- [145] G. Tononi, *BMC Neurosci.* **5**, 42 (2004).
- [146] S. Sarasso *et al.*, *Clin. EEG Neurosci.* **45**, 40 (2014).
- [147] M. Oizumi, L. Albantakis, and G. Tononi, *PLoS Comp. Biol.* **10**, e1003588 (2014).
- [148] H. Kim, A. G. Hudetz, J. Lee, G. A. Mashour, U. Lee, and the ReCCognition Study Group, *Front. Hum. Neurosci.*, **12**, 42 (2018).
- [149] M. Dhamala, G. Rangarajan, and M. Ding, *Phys. Rev. Lett.* **100**, 018701 (2008).
- [150] L. Ephremidze, G. Janashia, and E. Lagvilava, *Georgian Math. J.* **15**, 241 (2008).
- [151] L. Ephrimidze, F. Saied, and I. M. Spitkovsky, *IEEE Trans. Inform. Theor.* **64**, 728 (2018).
- [152] G. T. Wilson, *SIAM J. Appl. Math.* **23**, 420 (1972).
- [153] S. J. Luck and E. S. Kappenman (eds). *The Oxford Handbook of Event-Related Potential Components* (Oxford University Press, New York, NY, 2012).
- [154] K. J. Friston, L. Harrison, and W. Penny, *NeuroImage* **19**, 1273 (2003).
- [155] J. Courtiol, M. Guye, F. Bartolomei, S. Petkoski, and V. K. Jirsa, *J. Neurosci.* **40**, 5572 (2020).
- [156] V. K. Jirsa, T. Proix, D. Perdakis, M. M. Woodman, H. Wang, J. Gonzalez-Martinez, C. Bernard, C. Bénar, M. Guye, P. Chauvel, and F. Bartolomei, *NeuroImage* **145**, 377 (2017).
- [157] P. Sanz-Leon, S. A. Knock, A. Spiegler, and V. K. Jirsa, *NeuroImage* **111**, 385 (2015).
- [158] M. Steriade, *Neuroscience* **137**, 1087 (2006).